# 華中科技大學

## 本科生毕业设计（论文）参考文献译文本

译文出处：　Ryusuke Jinno and Masahiro Takimoto

Gravitational waves from bubble collision: analytic derivation

PHYSICAL REVIEW D 95, 024009 (2017)


院　　系　物理学院

专业班级　物理 1701

姓　　名　钟浩文

学　　号　U201713139

指导教师　龚碧平


2021 年 2 月

# 译文要求

一、 译文内容须与课题 (或专业内容) 联系，并需在封面注明详细出处。

二、 出处格式为

图书：作者. 书名. 版本（第 × 版）. 译者. 出版地：出版者，出版年. 起页 ～ 止页

期刊：作者. 文章名称. 期刊名称，年号，卷号（期号）：起页 ～ 止页

三、 译文不少于 5000 汉字（或 2 万印刷符）。

四、 翻译内容用五号宋体字编辑，采用 A4 号纸双面打印，封面与封底采用浅蓝色封面纸（卡纸）打印。要求内容明确，语句通顺。

五、 译文及其相应参考文献一起装订，顺序依次为封面、译文、文献。

六、 翻译应在第七学期完成。

# 译文评阅

**导师评语**

应根据学校“译文要求”，对学生译文翻译的准确性、翻译数量以及译文的文字表述情况等做具体的评价后，再评分。

评分:_____(百分制)　　指导教师(签名):_____

年　　月　　日

# Bubble 碰撞产生的引力波：解析推导

## 前言

我们在本文中讨论了宇宙学一阶相变过程中的 Bubble 碰撞产生的引力波。本文在采用所谓的薄壁近似 (Thin-Wall Approximation) 和包络近似 (Envelope Approximation) 的前提下通过分析 Bubble 产生、碰撞的动力学过程讨论了平坦时空背景下 Bubble 碰撞产生的引力波的能谱特征。我们发现能动张量的两点关联函数 $\langle T(x)T(y)\rangle$ 可以在这些假设下被解析得到并以此作为基础证明了 Bubble 碰撞过程中产生的引力波能谱本身也同样可以通过解析方式分析得到。虽然最后得到的能量密度谱的表达式仍然包含了两个不能被解析求解的积分，但是我们可以利用数值方法轻松得到具体的积分值。作为结论，我们发现整个物理过程中对于引力波能量谱的主要贡献来自于单一 Bubble 情形对能动张量两点关联函数的贡献，另外我们发现在高频波段引力波能量密度正比于 $f^{-1}$，在文章中我们也给出了相应的能谱拟合公式。

## 1 介绍

引力波 (GWs) 是众多被我们赋予厚望用以探测早期宇宙的手段之一。它们为我们研究暴涨时期的量子涨落、预加热、拓扑缺陷以及宇宙学相变 (PTs) 提供了一个独特的视角。值得一提的是，因为与超越粒子物理标准模型 (SM) 的高能物理关联紧密，早期宇宙经历的一阶相变长时间来一直备受人们的关注。事实上，在理论方面，已经有很多超越标准模型[1]的理论预言了宇宙学的一阶相变过程中会产生极其大量的引力波；在观测方面，地面的引力波探测器 KARGA, VIRGO 以及 Advanced LIGO 已经投入运行，空间引力波探测器例如 eLISA, BBO 以及 DECIGO 的实施计划也已经被提出。正是考虑到我们在未来探测到宇宙学起源的引力波的概率由于我们的探测手段的逐步提升而逐渐增大，从理论上对作为引力波宇宙学起源之一的相变引力波进行分析是非常有必要的。

宇宙学一阶相变通过 Bubble 的凝结、膨胀、碰撞以及热化为轻子而逐步进行，引力波正是在这一系列的过程中产生的。在相变的过程中，一部分被释放出来的能量用来加热等离子体，其余被释放出来的能量被一个可以用标量场描述的构型 (Bubble Wall) 以及/或者周围环境流体的总体运动而携带走。通过这样的局域能量释放而产生的引力波已经被一些基于薄壁近似和包络近似的文章通过数值求解的方法进行了研究。人们已经证明了这样的近似对于 Bubble 的能量主要源于标量场的构型的情况是适用的，最新的一些结果可以在参考文献【36】中得到。分析的方法是以一些对关联函数的假设为基础的。

在本文中，我们基于能动张量的两点关联函数 $\langle T(x)T(y)\rangle$ 对整个物理过程中产生的引力波进行了讨论，并且我们发现 $\langle T(x)T(y)\rangle$ 是用以计算得到引力波能量谱的唯一要素。我

[1]本文中提到的标准模型都指粒子物理标准模型而非宇宙学标准模型

们指出，在平直时空中辅助以薄壁近似和包络近似，对两点关联函数的计算可以得到一个相对简单的解析表达式，也正是因为如此，引力波的能量谱可以被解析地表达出来。虽然最后的能谱表达式仍然包含两个积分，但是它们可以通过数值方法轻松得到。我们提出的这种方法不仅仅避免了数值模拟方法不可避免的数值误差，并且可以帮助我们直接分析出对引力波能量谱贡献最大的特殊的 Bubble 构型。在目前阶段，我们的结果最符合例如近真空条件下的强相变情况，因为我们忽略了 Bubble 壁的有限厚度以及在 Bubble 碰撞之后的能动张量的局域结构事实上会在标量场和热等离子体强耦合的条件下变得十分重要的理论事实。但是我们的方法实际上可以推广到抛弃包络近似的一般情况下，这样的推广十分重要，并且会对我们理解 Bubble 碰撞之后的局域结构是如何产生引力波的提供巨大帮助。

本文的行文结构如下：在第二节中我们首先描述我们会采用的两个近似——薄壁近似以及包络近似，之后会介绍一些背景知识，比如运动方程以及引力波的能量谱。在第三节中我们给出了引力波能谱的解析表达式。因为最终仍有两个积分不能被显式求解，我们在第四节中给出了数值计算结果。我们在第五节中给出了考虑到有限速度（低于光速）的情况，并且在第六节中对全文进行了总结。

## 2 基本背景介绍

### 2.1 假设与近似

#### 2.1.1 薄壁近似与包络近似

在这一小节中，我们将介绍我们用来描述 Bubble 壁附近的能动张量的主要假设——薄壁近似和包络近似。

首先，我们将介绍薄壁近似——Bubble 所携带的所有能量都被认为局限在 Bubble 壁中，而 Bubble 壁的厚度被认为是无穷小的。为了计算的方便，我们令 Bubble 壁的厚度为 $l_B$。在这样的假设下我们可以将还没有发生碰撞的单个 Bubble 的能动张量设为：

$$T_{ij}^{B}(x) = \rho(x)\widehat{(x-x_N)}_i\widehat{(x-x_N)}_j \tag{2.1}$$

其中

$$\rho_x = \begin{cases} \dfrac{4\pi}{3} r_B(t)^3 \dfrac{\kappa\rho_0}{4\pi r_b(t)^2 l_B} & r_B(t) < |\boldsymbol{x}-\boldsymbol{x}_N| < r'_B \\ 0 & \text{其他情况} \end{cases} \tag{2.2}$$

$$r_B(t) = v(t-t_N) \qquad r'_B(t) = r_B(t) + l_B \tag{2.3}$$

这里我们定义 $x \equiv (t, \boldsymbol{x})$，带 $\wedge$ 的矢量 $\hat{\bullet}$ 代表沿着 $\vec{\bullet}$ 方向的单位矢量，$v$ 代表 Bubble 壁运动的速度，$\rho_0$ 代表在相变过程中释放出来的能量密度。[1]$\kappa$ 是一个效率因子，它决定了释放出来的能量密度被转化为局域在 Bubble 壁中的能量密度的比例。除此之外，本文中用拉丁字

[1]虽然对应的物理量是相变潜热并不是热环境中的能量密度，我们仍然在本文中采用“能量密度”这一描述。因为从 Bubble 碰撞过程中释放出的引力波与真空能远远大于热能对应的强相变更加相关。

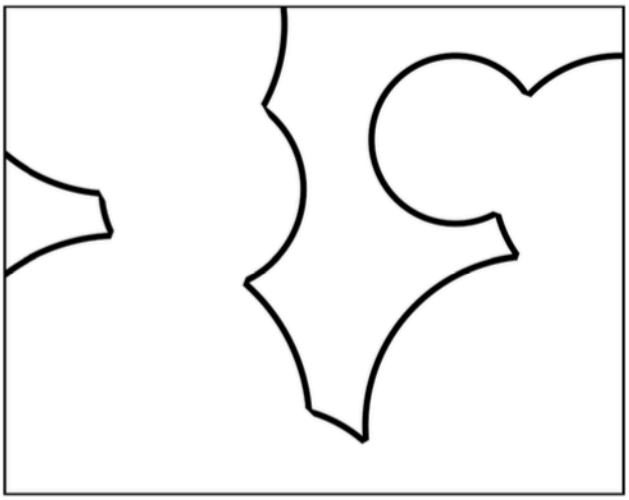

图 2-1　在包络近似下相变过程的简单描述。已经发生碰撞的 Bubble 壁不会作为引力波的波源，所有的时空点都只会被 Bubble 壁经过一次。

母表示的指标可以取遍 1，2，3。其次，我们认为 Bubble 壁的能动张量在发生碰撞之后的瞬间即为零 ($T = 0$)，在文献中这个假设被称为包络近似，在参考文献【28】中作者讨论了这种假设的合理性。图一给出了包络近似的简单描述。我们在之后会发现这两个假设大大简化了我们对引力波能谱的计算。值得一提的是，我们将那些与模型无关的物理量 $v, \rho_0, \kappa$ 认为是与时间无关的常量。

### 2.1.2　转化率

我们认为 Bubble 在单位时间单位体积内凝结的概率可以被写成如下形式：

$$\Gamma(t) = \Gamma_\star e^{\beta(t-t_\star)} \tag{2.4}$$

这里的 $t_\star$ 代表某一些相变发生时间点附近的固定的典型时间点，$\Gamma_\star$ 代表 $t = t_\star$ 时刻的凝结率，$\beta$ 被认为是一个常量。参数 $\beta$ 通常基于不同的物理模型利用顺子 (instanton) 方法进行计算，相变的典型持续时间 $\delta \sim \beta^{-1}$。我们认为相变过程持续的时间远远短于哈勃时间——$\beta/H \gg 1$，这一特征在通常的热力学相变中总是被满足的。

## 2.2　相变发生时的引力波功率谱

接下来我们将考虑如何将引力波的能量谱用能动张量的两点关联函数表示出来。

### 2.2.1　运动方程以及求解

在本文中我们考虑的引力波源自持续时间远小于哈勃时间的宇宙学一阶相变。对于这种情况，背景时空可以用闵氏时空很好地描述。在考虑张量微扰的情况下，我们可以将背景

时空的度规写成如下形式：

$$ds^2 = -dt^2 + (\delta_{ij} + 2h_{ij})dx^i dx^j \tag{2.5}$$

张量微扰满足横向无迹条件：$h_{ii} = \partial_j h_{ij} = 0$ 并且满足如下运动方程：

$$\ddot{h}_{ij}(t, \boldsymbol{k}) + k^2 h_{ij}(t, \boldsymbol{k}) = 8\pi G \Pi_{ij}(t, \boldsymbol{k}) \tag{2.6}$$

这里的 $G$ 是牛顿万有引力常数，$\bullet(t, \boldsymbol{k})$ 表示波矢 $\boldsymbol{k}$ 对应的傅立叶模式。这里采用传统的傅立叶变换的定义 $\int d^3x e^{i\boldsymbol{k}\cdot\boldsymbol{x}}$ 以及 $\int d^3k/(2\pi)^3 e^{-i\boldsymbol{k}\cdot\boldsymbol{x}}$。$\Pi_{ij}$ 是能动张量的横向无迹投影部分：

$$\Pi_{ij}(t, \boldsymbol{k}) = K_{ij,kl}(\boldsymbol{k}) T_{kl}(t, \boldsymbol{k}) \tag{2.7}$$

其中 $T_{ij}$ 是能动张量，$K_{ij,kl}$ 称为投影张量：

$$K_{ij,kl}(\boldsymbol{k}) = P_{ik}(\boldsymbol{k}) P_{jl}(\boldsymbol{k}) - \frac{1}{2} P_{ij}(\boldsymbol{k}) P_{kl}(\boldsymbol{k}) \tag{2.8}$$

$$P_{ij}(\boldsymbol{k}) = \delta_{ij} - \boldsymbol{k}_i \boldsymbol{k}_j \tag{2.9}$$

这里我们认为波源项存在于 $t_{\text{start}}$ 到 $t_{\text{end}}$ 之间，并且我们在最后计算的时候设 $t_{\text{start/end}} \to \mp\infty$。式 (2.6) 的解可以用满足 $G_k(t,t) = 0, \partial G_k(t,t')/\partial t|_{t=t'} = 1$ 的格林函数表示：

$$h_{ij}(t, \boldsymbol{k}) = 8\pi G \int_{t_{\text{start}}}^{t} dt' G_k(t, t') \Pi_{ij}(t', \boldsymbol{k}) \qquad t < t_{\text{end}} \tag{2.10}$$

这里的 $G_k(t,t') = \sin(k(t - t_{\text{end}}))$, 对于 $t > t_{\text{end}}$ 的情形，我们可以利用在 $t = t_{\text{end}}$ 时候的连接条件给出

$$h_{ij}(t, \boldsymbol{k}) = \mathcal{A}_{ij}(\boldsymbol{k}) \sin\Big[k(t - t_{end})\Big] + \mathcal{B}_{ij}(\boldsymbol{k}) \cos\Big[k(t - t_{end})\Big] \tag{2.11}$$

其中两个系数 $\mathcal{A}$ 和 $\mathcal{B}$ 的具体形式如下

$$\mathcal{A}_{ij}(\boldsymbol{k}) = \frac{8\pi G}{k} \int_{t_{start}}^{t_{end}} dt \cos\Big[k(t_{end} - t)\Big] \Pi_{ij}(t, \boldsymbol{k}) \tag{2.12}$$

$$\mathcal{B}_{ij}(\boldsymbol{k}) = \frac{8\pi G}{k} \int_{t_{start}}^{t_{end}} dt \sin\Big[k(t_{end} - t)\Big] \Pi_{ij}(t, \boldsymbol{k}) \tag{2.13}$$

### 2.2.2 功率谱

下面我们将会借助式 (2.11) 来表示引力波能量谱。我们首先定义等时关联函数

$$\langle \dot{h}_{ij}(t, \boldsymbol{k}) \dot{h}_{ij}(t, \boldsymbol{q}) \rangle := (2\pi)^3 \delta^{(3)}(\boldsymbol{k} - \boldsymbol{q}) P_{\dot{h}}(t, k) \tag{2.14}$$

同时定义波源项非等时关联函数

$$\langle \Pi_{ij}(t_x, \boldsymbol{k}) \Pi_{ij}(t_y, \boldsymbol{q}) \rangle := (2\pi)^3 \delta^{(3)}(\boldsymbol{k} - \boldsymbol{q}) \Pi(t_x, t_y, k) \tag{2.15}$$

这里的尖括号 $\langle ... \rangle$ 表示系综平均。注意到式 (2.15) 中出现了 $(2\pi)^3 \delta^{(3)}(\boldsymbol{k} - \boldsymbol{q})$，这一项的出现源自于我们讨论的系统具有空间上的均匀性。在有了原始的能动张量的表达式的基础上，

我们可以将关联函数改写如下：

$$\Pi(t_x,t_y,k)=K_{ij,kl}(\boldsymbol{k})K_{ij,mn}(\boldsymbol{k})\int d\boldsymbol{r}e^{i\boldsymbol{k}\cdot\boldsymbol{r}}\langle T_{kl}T_{mn}\rangle(t_x,t_y,\boldsymbol{r}) \tag{2.16}$$

这里我们用了一个简记

$$\langle T_{kl}T_{mn}\rangle(t_x,t_y,\boldsymbol{r})\equiv\langle T_{kl}(t_x,\boldsymbol{x})T_{mn}(t_y,\boldsymbol{y})\rangle \tag{2.17}$$

这里有 $\boldsymbol{r}\equiv\boldsymbol{x}-\boldsymbol{y}$。上式的左边由于我们认为空间是均匀的因此仅仅依赖于 $\boldsymbol{r}$。现在让我们考虑 $t>t_{\text{end}}$ 的情况。由于引力波以及波源项由式 (2.11) 互相联系，我们可以将功率谱 $P_{\dot{h}}(t,k)$ 写成如下形式：[1]

$$P_{\dot{h}}(t,k)=32\pi^2G^2\int_{t_{start}}^{t_{end}}dt_x\int_{t_{start}}^{t_{end}}dt_y\cos\Big[k(t_x-t_y)\Big]\Pi(t_x,t_y,k) \tag{2.18}$$

虽然我们在 (2.18) 式的左边将 $t$ 也作为一个功率谱 $P_{\dot{h}}(t,k)$ 所依赖的参数，但是实际上在 $t>t_{\text{end}}$ 时并不存在波源项同时我们忽略了宇宙的膨胀，因此等式右边是不会依赖于时间 $t$ 的。引力波的总的能量密度可以写成如下形式：

$$\rho_{gw}(t)=\frac{\langle\dot{h}_{ij}(t,\boldsymbol{x})\dot{h}_{ij}(t,\boldsymbol{x})\rangle_T}{8\pi G} \tag{2.19}$$

这里的 $\langle...\rangle_T$ 表示对振动的平均 (对时间求平均) 以及系综平均，因此单位对数频率内的引力波能量密度可以表示成如下形式：

$$\Omega_{GW}(t,k):=\frac{1}{\rho_c}\frac{d\rho_{GW}}{d\log k}=\frac{2Gk^3}{\pi\rho_c}\int_{t_{start}}^{t_{end}}dt_x\int_{t_{start}}^{t_{end}}dt_y\cos\Big[k(t_x-t_y)\Big]\Pi(t_x,t_y,k) \tag{2.20}$$

这里的 $\rho_{tot}$ 是宇宙的总能量密度。那么到此为止，我们要做的就是通过分析 $\Pi(t_x,t_y,k)$ 或者说通过分析能动量张量的两点关联函数 $\langle T(x)T(y)\rangle$ 来分析引力波的能量密度谱。一旦我们建立了一个合理的模型，我们原则上就可以解析地分析这些物理量。事实上，在本文的后半部分我们将会看到能动量张量的两点关联函数在薄壁近似和包络近似下确实是可以得到解析的表达式的。

为了后续分析的方便，我们现在将引力波谱的形式重新改写如下。为此，我们需要再定义物理量 $\alpha$ 如下

$$\alpha:=\frac{\rho_0}{\rho_{rad}}\quad\rho_{tot}=\rho_0+\rho_{rad} \tag{2.21}$$

$\alpha$ 描述了相变过程中释放出来的能量密度与辐射能量密度的比值。这里 $\rho_{tot}$ 和 $\rho_{rad}$ 是宇宙的总能量密度以及辐射能量密度[2]。利用如上定义我们可以将引力波的能量密度重新改写如

[1]原文计算有误，事实上还漏了一项在做了时间平均后为零的项，具体形式为

$$32\pi^2G^2\int_{t_{start}}^{t_{end}}dt_x\int_{t_{start}}^{t_{end}}dt_y\cos\Big[k(2t-t_x-t_y)\Big]\Pi(t_x,t_y,k)$$

[2]注意区分这里的辐射能量密度和引力辐射的能量密度，由于这是极早期宇宙，是一个辐射主导 (radiation-dominated) 的宇宙，因此我们考虑宇宙的能量只需要考虑辐射的贡献。

下：

$$\Omega_{GW}(t,k)=\kappa^2\left(\frac{H_*^2}{\beta}\right)^2\left(\frac{\alpha}{1+\alpha}\right)^2\Delta(k/\beta,v) \tag{2.22}$$

其中的 $\Delta$ 由下式给出

$$\Delta(k/\beta,v)=\frac{3}{4\pi^2}\frac{\beta^2k^3}{\kappa^2\rho_0^2}\int_{t_{start}}^{t_{end}}dt_x\int_{t_{start}}^{t_{end}}dt_y\cos\Big[k(t_x-t_y)\Big]\Pi(t_x,t_y,k) \tag{2.23}$$

在得到式 (2.22) 的过程中我们已经利用了弗里德曼方程 $H_\star^2=(8\pi G/3)\rho_{tot}$，其中 $H_\star$ 为相变发生时刻的哈勃常数。我们注意到 $\Delta$ 仅仅依赖于 $k/\beta$ 以及 Bubble 壁的运动速度 $v$。因为我们在式 (2.22) 中已经将与模型无关的常量 $\kappa,\rho_0$ 提到了 $\Delta$ 外，因此我们可以发现 $\Delta$ 本身是一个无量纲的物理量。

### 2.3 现在的引力波功率谱

在引力波产生之后，它就在传播过程中经历了宇宙学红移。我们知道相变产生时的尺度因子 $a_\star$ 以及目前的尺度因子 $a_0$ 的关系由下式给出：

$$\frac{a_0}{a_*}=8.0\times10^{-16}\left(\frac{g_*}{100}\right)^{-1}\left(\frac{T_*}{100\text{GeV}}\right)^{-1} \tag{2.24}$$

其中 $T_\star$ 代表相变发生时的温度，$g_\star$ 代表温度为 $T_\star$ 时的宇宙的总的相对论性的等效自由度 (relativistic degree of freedom)。根据尺度因子的变换关系，我们可以得到引力波频率的变换关系如下

$$f=f_*\left(\frac{a_*}{a_0}\right)=1.65\times10^{-5}\text{Hz}\left(\frac{f_*}{\beta}\right)\left(\frac{\beta}{H_*}\right)\left(\frac{T_*}{100\text{GeV}}\right)\left(\frac{g_*}{100}\right)^{1/6} \tag{2.25}$$

注意到引力波是一种近似与其他物质没有作用的辐射我们可以得到目前的引力波能量密度满足[1]

$$\Omega_{GW}h^2=1.67\times10^{-5}\kappa^2\Delta\left(\frac{\beta}{H_*}\right)^{-2}\left(\frac{\alpha}{1+\alpha}\right)^2\left(\frac{g_*}{100}\right)^{-1/3} \tag{2.26}$$

## 3 解析表达式

这一节内容的主要目的是为了得到 $\Delta$ 的具体表达式。首先我们考虑 Bubble 壁以光速运动的情况，我们会看到这种情况的结果比较简单。在得到这种简单情况结果之后对 $v\neq c$ 情况的推广是直截了当的，我们会在第五节讨论这个问题。

由式 (2.23) 给出的引力波能量密度谱中唯一非平庸的物理量就是由 (2.16) 给出的两点关联函数。如果我们可以计算这个物理量或者计算等价的物理量——给定 $t_x,t_y,\boldsymbol{r}=\boldsymbol{x}-\boldsymbol{y}$ 情况下的能动张量乘积的系综平均 $\langle T_{ij}T_{kl}\rangle(t_x,t_y,\boldsymbol{r})$，我们就可以得到引力波的能量密度谱。下面我们就会逐步给出计算证明这是完全有可能的。为了使得能动张量在 $x=(t_x,\boldsymbol{x})$ 以及 $y=(t,\boldsymbol{y})$ 这两个时空点的值不为零，需要满足如下两个条件：

[1] 这里要注意 $h$ 是无量纲的哈勃常数而不是微扰度规

- 在 $x, y$ 两个时空点的过去光锥内部不存在 Bubble 凝结
- Bubble 恰好在 $x, y$ 两点的过去光锥上凝结，因此可以使得 Bubble 壁在 $t_x$ 时刻经过 $\boldsymbol{x}$，在 $t_y$ 时刻经过 $\boldsymbol{y}$

为了理解上述的两个条件，读者需要注意到任何一个空间点在包络近似下都只能被 Bubble 壁经过一次。那么如果存在 Bubble 在 $x, y$ 两点的过去光锥内凝结，那么总有一个点早在 $t_x$ 或者 $t_y$ 之前已经被 Bubble 壁经过了。那么这样就不可能满足我们之前要求的在 $x, y$ 两点的能动张量值非零。另一方面，让 Bubble 恰好在 $x, y$ 两点的过去光锥上凝结是让 Bubble 壁恰好在对应时间经过对应空间点的必要条件。不过这里要注意，事实上这里一共有两种可能的情况：经过 $x, y$ 两个时空点的 Bubble 壁属于同一个凝结点产生的 Bubble 或者是分属于两个不同凝结点产生的不同 Bubble。我们称这两种情况分别为单一 Bubble 情况以及双生 Bubble 情况。图 3-1 简单描述了这两种不同的情况对关联函数 $\langle T(x)T(y)\rangle$ 的贡献。这里读

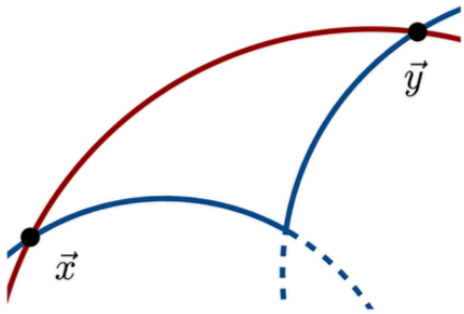


图 3-1　单一 Bubble 以及双生 Bubble 情形对两点关联函数 $\langle T(x)T(y)\rangle$ 的贡献简图。其中红线对应了单一 Bubble 情形，而蓝线对应双生 Bubble 情形。图中虚线部分在包络近似下可以忽略。注意到，虽然这幅图出于方便考虑仅仅展示了 $t_x = t_y$ 的情形，但是实际上来自于 $t_x \neq t_y$ 的情形也会在计算两点关联函数的时候做出贡献。

者可能会产生一个疑问，为什么单一的 Bubble 也会对引力波的产生做出贡献呢？众所周知球对称分布的质量结构不会辐射出引力波。这里的关键在于单一 Bubble 情形实际上是将球对称结构的破缺考虑在内的，通过 Bubble 的碰撞球对称结构自然就消失了，具体分析可以参考附录 B。

在下面的讨论中我们明确我们所采用的记号，其次在讨论了在 $x, y$ 两点过去光锥内不存在 Bubble 凝结的条件之后我们分开讨论单一 Bubble 和双生 Bubble 的情形。最终的表达式由式 (3.54) 和 (3.63) 给出，对于那些仅仅需要最终引力波能量谱的读者直接跳转到第 4 节即可。

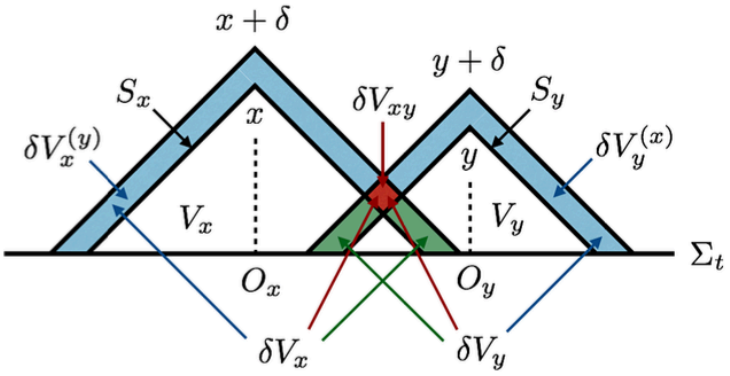


图 3-2　位于 $x, y$ 两点过去光锥上的物理量的记号示意

### 3.1　记号

我们首先明确我们在之后的论述中会用到的记号和一些规范。我们将两点关联函数中讨论的两个时空点分别记为

$$x := (t_x, \boldsymbol{x}) \qquad y := (t_y, \boldsymbol{y}) \tag{3.1}$$

我们之后也会用到两个不同的时间参量 $T, t_d$，它们的具体定义如下

$$T := \frac{t_x + t_y}{2} \qquad t_d := t_x - t_y \tag{3.2}$$

除了时间变量之外，我们同样定义空间间隔

$$\boldsymbol{r} := \boldsymbol{x} - \boldsymbol{y} \qquad r := |\boldsymbol{r}| \tag{3.3}$$

我们会一直讨论 $x, y$ 的过去光锥，我们将它们分别记为 $S_x, S_y$。包含在 $S_x, S_y$ 之内的部分被记为 $V_x, V_y$，同时我们记两者的并集为 $V_{xy} = V_x \cup V_y$。由于我们讨论的 Bubble 壁的厚度为 $l_B$，因此我们还需要定义两个时空点

$$x + \delta := (t_x + l_B, \boldsymbol{x}) \qquad y + \delta := (t_y + l_B, \boldsymbol{y}) \tag{3.4}$$

这两个时空点的过去光锥分别被记为 $S_{x+\delta}$ 以及 $S_{y+\delta}$。我们同样定义如下时空区域为

$$\delta V_x := V_{x+\delta} - V_x \qquad \delta V_y := V_{y+\delta} - V_y \tag{3.5}$$

以及它们两者的交集为

$$\delta V_{xy} := \delta V_x \cap \delta V_y \tag{3.6}$$

另外我们也定义

$$\delta V_x^{(y)} := \delta V_x - V_{y+\delta} \qquad \delta V_y^{(x)} := \delta V_y - V_{x+\delta} \tag{3.7}$$

这些物理量在图 3-2，图 3-3 中直观地画出。在图 3-3 中我们展示了图 3-2 中的物理图像在 2+1 维时空中的图像。

我们考虑某一个时间为 $t$ 的等时超曲面 $\Sigma_t$，两个过去光锥 $S_x$ 和 $S_y$ 如图 3-4 所示形成了两个球体。我们称这两个球体分别为 $C_x(t)$ 和 $C_y(t)$，它们的球心分别被记为 $O_x$ 和 $O_y$。

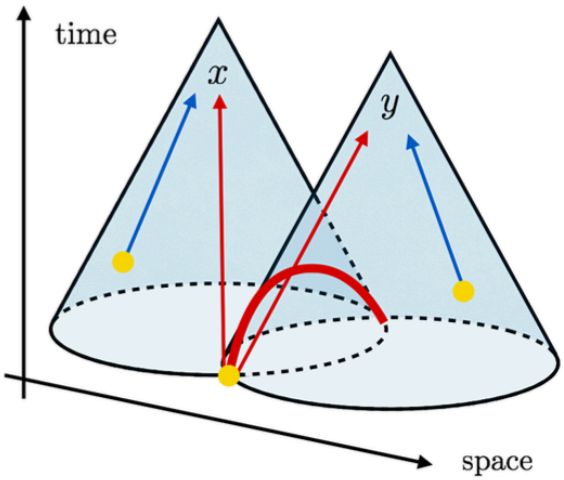


图 3-3　图 3-2 中的过去光锥在 2+1 维时空中的立体图像。其中黄色的圆形代表 Bubble 的凝结点，红色箭头代表单一 Bubble 情形的贡献，蓝色箭头代表双生 Bubble 情形的贡献。其中沿着两圆锥相交部分延展的红线部分就代表着图 3-2 中的 $\delta V_{xy}$

两个球体的半径如下：

$$r_x(t) := t_x - t \qquad r_y(t) := t_y - t \tag{3.8}$$

这两个球体会在 $t < t_{xy}$ 时有一个交集，而 $t_{xy}$ 由下式给出：

$$t_{xy} := \frac{t_x + t_y - r}{2} \tag{3.9}$$

下面让我们考虑球体 $C_x(t)$ 和 $C_y(t)$ 上的任意两个点 $P_x(t)$ 和 $P_y(t)$，我们记从 $O_x$ 和 $O_y$ 指向 $P_x(t)$ 和 $P_y(t)$ 的单位矢量分别为 $n_x(t)$ 和 $n_y(t)$。我们用方位角和极角来描述这两个单位矢量

$$n_x \equiv \left\{ s_x c_{\phi x}, s_x s_{\phi x}, c_x \right\} \quad n_y \equiv \left\{ s_y c_{\phi y}, s_y s_{\phi y}, c_y \right\} \tag{3.10}$$

为了书写方便，这里已经省略了时间 $t$。同时我们也采用了简记 $c_x(s_x) \equiv \cos\theta_x(\sin\theta_x)$，以及 $c_{\phi x}(s_{\phi x}) \equiv \cos\phi_x(\sin\phi_x)$ 其他记号以此类推。我们之后也会需要标记处于 $C_x(t)$ 和 $C_y(t)$ 交集中的点，我们将这些点记为 $P(t)$，并且将从 $O_x$ 和 $O_y$ 指向这些点的单位矢量分别记为 $n_{x\times}(t)$ 和 $n_{y\times}(t)$。这些单位矢量同样可以用方位角和极角 $\theta_{x\times}(t), \theta_{y\times}(t), \phi_{x\times}(t), \phi_{y\times}(t)$ 描述。特别的是，我们可以给出极角的余弦如下：

$$c_{x\times}(t) = \cos\theta_{x\times}(t) = -\frac{r_x(t)^2 + r^2 - r_y(t)^2}{2r_x(t)r} \tag{3.11}$$

$$c_{y\times}(t) = \cos\theta_{y\times}(t) = \frac{r_y(t)^2 + r^2 - r_x(t)^2}{2r_y(t)r} \tag{3.12}$$

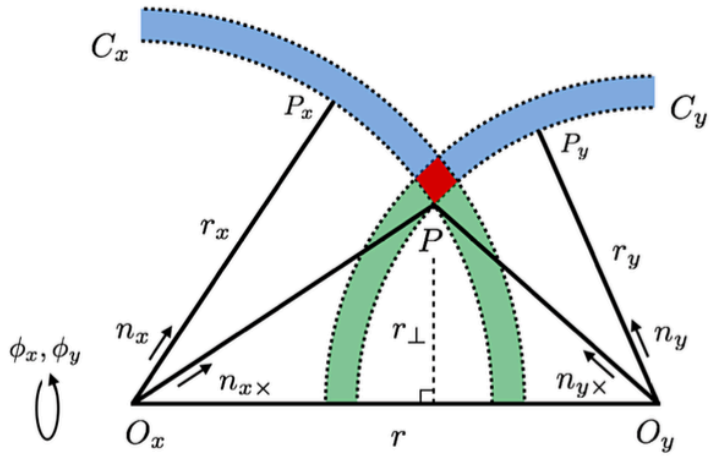


图 3-4　在等时超曲面 $\Sigma_t$ 上的相关物理量的说明图。红色的菱形状区域代表在单一 Bubble 情形中 Bubble 凝结的区域，而蓝色的区域代表双生 Bubble 情形中 Bubble 凝结的区域。

## 3.2　时空点处于假真空的概率

### 3.2.1　单个时空点处于假真空态的概率

为了论证更加容易理解，我们首先考虑单个时空点 $x$ 处于假真空态的概率 $P(x)$。这种情况当且只当 $V_x$ 中没有 Bubble 凝结的时候才会出现。我们将 $V_x$ 分割为无穷多个无穷小的四维体元 $dV_x^i$ 所以就有 $V_x = \cup_i dV_x^i$，没有 Bubble 在 $dV_x^i$ 内凝结的概率由 $(1 - \Gamma dV_x^i)$ 给出。因此 $P(x)$ 可以写成如下形式：

$$P(x) = \prod_i^\infty \left(1 - \Gamma dV_x^i\right) \tag{3.13}$$

其中

$$I(x) = \int_{V_x} d^4 z \Gamma(z) \tag{3.14}$$

### 3.2.2　两个时空点都处于假真空态的概率

下面让我们来考虑给定的两个时空点 $x$ 以及 $y$ 同时处于假真空态的概率 $P(x, y)$。这个概率可以表示如下：

$$P(x,y) = e^{-I(x,y)} \qquad I(x,y) = \int_{V_{xy}} d^4\Gamma(z) \tag{3.15}$$

在下面的计算中我们只考虑 $x, y$ 两点间隔为类空间隔——$r > |t_x - t_y|$，因为只有这样的构型才在包络近似下对我们计算引力波的波谱有贡献。于是 $I(x, y)$ 就可以被写成如下形式：

$$I(x,y) \equiv I_x^{(y)} + I_y^{(x)} \tag{3.16}$$

$$I_x^{(y)} = \int_{-\infty}^{t_{xy}} dt \frac{\pi}{3} r_x(t)^3 \Gamma(t) \Big(2 - c_{x\times}(t)\Big) \Big(1 + c_{x\times}(t)\Big)^2 + \int_{t_{xy}}^{t_x} dt \frac{4\pi}{3} r_x(t)^3 \Gamma(t) \tag{3.17}$$

$$I_y^{(x)} = \int_{-\infty}^{t_{xy}} dt \frac{\pi}{3} r_y(t)^3 \Gamma(t) \Big(2 + c_{y\times}(t)\Big)\Big(1 - c_{y\times}(t)\Big)^2 + \int_{t_{xy}}^{t_y} dt \frac{4\pi}{3} r_y(t)^3 \Gamma(t) \tag{3.18}$$

这里我们发现在 $t \in [-\infty, t_{xy}]$ 和其他不同的时间区间，被积函数的具体形式是不同的。这是因为在前一个时间区间内积分区域并不形成完整的球体，具体的积分结果由下式给出：

$$I(x,y) = 8\pi\Gamma(T)\mathcal{I}(t_d, r) \tag{3.19}$$

$$\mathcal{I}(t_d, r) = e^{t_d/2} + e^{-t_d/2} + \frac{t_d^2 - (r^2+4r)}{4r} e^{-r/2} \tag{3.20}$$

这里我们将参数 $(t_x, t_y)$ 转化为了 $(T, t_d)$，并且在不失一般性的前提下令 $\beta = 1$。

### 3.3 单一 Bubble 的波谱

下面我们开始计算单一 Bubble 情形时式 (2.16) 中的两点关联函数。在包络近似下只有满足如下两条条件才有可能使得单一 Bubble 在 $x, y$ 两点可以提供非零的能动张量：

- 在 $V_{xy}$ 内没有 Bubble 凝结产生
- 至少有一个 Bubble 在 $\delta V_{xy}$ 内凝结产生

注意到最后一个条件在薄壁近似 ($l_B \to 0$) 的前提下会演变为“仅仅有一个 Bubble 在 $\delta V_{xy}$ 内凝结产生”。下面我们在以上两个条件的前提下简单推导单一 Bubble 情况下的引力波波谱。最后的形式由式 (54) 给出，具体的计算细节可以参考附录 A。

在以上考虑的基础上，我们发现单一 Bubble 情况下对能动张量的贡献可以写成如下的形式（“$s$”是 single 的缩写，代表单一 Bubble 情形。）

$$\langle T_{kl} T_{mn} \rangle^{(s)}(t_x, t_y, \boldsymbol{r}) = P(t_x, t_y, r) \int_{-\infty}^{t_{xy}} dt_n \Gamma(t_n) \mathcal{T}^{(s)}_{ij,kl}(t, t_x, t_y, \boldsymbol{r}) \tag{3.21}$$

这里的 $\mathcal{T}^{(s)}_{ij,kl}$ 是在在 $t_n$ 时刻凝结的 Bubble 壁的 $T_{ij}(x)T_{kl}(y)$ 的值 (具体可以参考图 3-2 和图 3-3)。具体可以计算如下：

$$\mathcal{T}^{(s)}_{ij,kl} = \left(\frac{4\pi}{3} r_x(t_n)^3 \cdot \kappa\rho_0 \cdot \frac{1}{4\pi r_x(t_n)^2 \ell_B}\right) \times \left(\frac{4\pi}{3} r_y(t_n)^3 \cdot \kappa\rho_0 \cdot \frac{1}{4\pi r_y(t_n)^2 \ell_B}\right) \times \int_{R_{xy}} d^3 z \Big(N_x\Big)_{ijkl} \tag{3.22}$$

其中 $\Big(N_x\Big)_{ijkl} \equiv (n_{x\times})_i (n_{x\times})_j (n_{y\times})_k (n_{y\times})_l$。这里的 $R_{xy} \equiv \delta V_{xy} \cap \Sigma_{t_n}$ 是图 $3-4$ 中的菱形结构绕着 $\boldsymbol{r}$ 轴旋转一周而成的环。式 (47) 的结果可以直接给出，之后我们再做横向无迹投影乘上以式 (16) 给出的投影算子 $K$，我们可以得到如下结果：

$$K_{ij,kl}(\boldsymbol{k}) K_{ij,mn}(\boldsymbol{k}) \langle T_{kl} T_{mn} \rangle^{(s)}(t_x, t_y, \boldsymbol{r}) = \frac{2\pi}{9} \kappa^2 \rho_0^2 P(t_x, t_y, r)^\Gamma(T) \frac{e^{-r/2}}{r^5} \left[\frac{1}{2} F_0 + \frac{1}{4}(1 - c_{rk}^2) F_1 + \frac{1}{16}(1 - c_{rk}^2) F_2\right] dt_n \tag{3.23}$$

其中

$$F_0 = 2(r^2 - t_d^2)^2(r^2 + 6r + 12) \tag{3.24}$$

$$F_1 = 2(r^2 - t_d^2)\Bigg[ - r^2(r^3 + 4r^2 + 12r + 24) + t_d^2(r^3 + 12r^2 + 60r + 120)\Bigg] \tag{3.25}$$

$$F_2 = \frac{1}{2}\Bigg[r^4(r^4 + 4r^3 + 20r^2 + 72r + 144) - 2t_d^2 r^2(r^4 + 12r^3 + 84r^2 + 360r + 720) + t_d^4(r^4 + 20r^3 + 180r^2 + 840r = 1680)\Bigg] \tag{3.26}$$

注意到这里我们已经将时间变量从 $(t_x, t_y)$ 转变为了 $(T, t_d)$。并且我们注意到至此关联函数就已经可以被解析地表达出来了。下面我们通过对 $\boldsymbol{r}$ 和 $\boldsymbol{k}$ 的夹角进行积分就可以得到如下结果：

$$\Pi^{(s)}(t_x, t_y, k) = \frac{4\pi^2}{9}\kappa^2\rho_0^2\Gamma(T)\int_0^\infty dr\frac{e^{-r/2}}{r^3}P(t_x, t_y, r) \times \left[j_0(kr)F_0 + \frac{j_1(kr)}{kr}F_1 + \frac{j_2(kr)}{k^2r^2}F_2\right] \tag{3.27}$$

之后我们需要对时间 $T$ 的积分，我们利用了如下的恒等式：$\int_{-\infty}^{+\infty} dY e^{-Xe^Y + nY} = (n-1)!/X^n$ 于是我们可以得到：

$$\Delta^{(s)} = \frac{k^3}{12\pi}\int_0^{+\infty}\int_{r_d}^{+\infty}\frac{e^{-r/2}\cos(kt_d)}{r^3\mathcal{I}(t_d, r)}\left[j_0(kr)F_0 + \frac{j_1(kr)}{kr}F_1 + \frac{j_2(kr)}{k^2r^2}F_2\right] \tag{3.28}$$

### 3.4 双生 Bubble 的波谱

下面我们开始考虑双生 Bubble 情况下对关联函数的贡献。在包络近似的前提下，如果要求再 $x, y$ 两点的能动张量的值非零，下面的两个条件是必要的。

- 在 $V_{xy}$ 内没有 Bubble 凝结
- 至少有一个 Bubble 在 $\delta V_x^{(y)}$ 凝结并且至少有一个 Bubble 在 $\delta V_y^{(x)}$ 凝结。

注意到在薄壁近似下就简化为了有且仅有一个 Bubble 在 $\delta V_x^{(y)}$ 凝结，并且有且仅有一个 Bubble 在在 $\delta V_y^{(x)}$ 凝结。下面我们就将在这两个条件的基础上推导得到双生 Bubble 情形下的引力波波谱的具体形式。最终的结果由式 (63) 给出。

在有了以上的考虑之后，双生 Bubble 对于能动张量的贡献可以分解为如下形式（“$d$” 是 double 的缩写，代表双生 Bubble 情形)

$$\begin{aligned}\langle T_{ij}T_{kl}\rangle^{(d)}(t_x, t_y, \boldsymbol{r}) \quad = \quad & P(t_x, t_y, r) \\ & \times \int_{-\infty}^{t_{xy}} dt_{xn}\Gamma(t_{xn})\int_{\delta V_x^{(y)}\cap\Sigma_{txn}} d^3x_n\mathcal{T}_{x,ij}^{(d)}(t_{xn}, \boldsymbol{x}; t_x, \boldsymbol{r}) \\ & \times \int_{-\infty}^{t_{xy}} dt_{yn}\Gamma(t_{yn})\int_{\delta V_y^{(x)}\cap\Sigma_{tyn}} d^3y_n\mathcal{T}_{y,kl}^{(d)}(t_{yn}, \boldsymbol{y}; t_y, \boldsymbol{r})\end{aligned} \tag{3.29}$$

这里的 $\mathcal{T}_{x,ij}^{(d)}$ 和 $\mathcal{T}_{y,kl}^{(d)}$ 是两个分别在 $\delta V_x^{(y)} \cap \Sigma_{txn}$ 以及 $\delta V_y^{(x)} \cap \Sigma_{tyn}$ 内凝结的 Bubble 在时空点

$x$ 和 $y$ 处的能动张量的值。它们的具体形式由下两式给出

$$\mathcal{T}^{(d)}_{x,ij}(t_{xn},\boldsymbol{x};t_x,\boldsymbol{r})=\left(\frac{4\pi}{3}r_x(t_{xn})^3\cdot\kappa\rho_0\cdot\frac{1}{4\pi r_x(t_{xn}^2 l_B)}\right)(n_x)_i(n_x)_j \tag{3.30}$$

$$\mathcal{T}^{(d)}_{y,kl}(t_{yn},\boldsymbol{y};t_y,\boldsymbol{r})=\left(\frac{4\pi}{3}r_y(t_{yn})^3\cdot\kappa\rho_0\cdot\frac{1}{4\pi r_y(t_{yn}^2 l_B)}\right)(n_y)_k(n_y)_l \tag{3.31}$$

这里的参数 $t_{xn},t_{yn}$ 已经为了方便而省略了。注意到在式 (3.29) 中的时间积分区间为 $(-\infty,t_{xy}]$，要理解这一点我们要注意到在 $t_{xn}>t_{xy}$ 以及 $t_{yn}>t_{xy}$ 时已经形成了完整的球体，因此这种情况拥有球对称性导致它们的贡献为零。(参考图 3-4，我们可以注意到 $P_x,P_y$ 可以取遍完整的球体)。同时我们要注意到在 (3.29) 式中对于 $x$ 和 $y$ 两点的贡献是分开计算的，这是由于两个 Bubble 是独立凝结的。注意到这个系统中除了 $\boldsymbol{r}$ 之外不存在其他特殊的方向，因此 $\mathcal{T}^{(d)}_{z,ij}(z=x,y)$ 可以被分解如下：

$$\int_{-\infty}^{t_{xy}}dt_{zn}\Gamma(t_{zn})\int d^3z_n\mathcal{T}^{(d)}_{z,ij}(t_{zn},\boldsymbol{z}_n;t_z,\boldsymbol{r})=\mathcal{A}^{(d)}_z(t_x,t_y,r)\delta_{ij}+\mathcal{B}^{(d)}_z(t_x,t_y,r)\hat{r}_i\hat{r}_j \tag{3.32}$$

这里的 $\mathcal{A}^{(d)}_z$ 和 $\mathcal{B}^{(d)}_z$ 同时依赖于 $t_x,t_y$，因为具体的积分区域是同时依赖于两个点的。我们可以注意到上式在投影算子 $K$ 的作用下仅仅有与 $\mathcal{B}$ 相关的量有非零的贡献：

$$K_{ij,kl}(\hat{k})K_{ij,mn}(\hat{k})\langle T_{kl}T_{mn}\rangle^{(d)}(t_x,t_y,\boldsymbol{r})=\frac{1}{2}P(t_x,t_y,r)\mathcal{B}^{(d)}_x\mathcal{B}^{(d)}_y\left[1-(\hat{r}\cdot\hat{k})^2\right]^2 \tag{3.33}$$

不失一般性地我们可以令 $\beta=1$，并且计算 $\mathcal{B}$ 得到如下结果：

$$\mathcal{B}^{(d)}_x(t_x,t_y,r)=-\frac{\pi}{6}\kappa\rho_0\frac{e^{-r/2}}{r^3}\Gamma(T)G(t_d,r) \tag{3.34}$$

$$\mathcal{B}^{(d)}_y(t_x,t_y,r)=-\frac{\pi}{6}\kappa\rho_0\frac{e^{-r/2}}{r^3}\Gamma(T)G(-t_d,r) \tag{3.35}$$

这里的方程 $G$ 由下式给出：

$$G(t_d,r)=(r^2-t_d^2)\left[(r^3+2r^2)+t_d(r^2+6r+12)\right] \tag{3.36}$$

注意到这里我们实际上已经将关联函数解析地表达了出来。正如在单一 Bubble 情形中一样，在这里我们同样可以积分得到：

$$\Pi^{(d)}(t_x,t_y,k)=\frac{4\pi^3}{9}\kappa^2\rho_0^2\Gamma(T)^2\int_0^\infty drP(t_x,t_y,r)\frac{e^{-r}}{r^4}\times\frac{j_2(kr)}{k^2r^2}G(t_d,r)G(-t_d,r) \tag{3.37}$$

将该式重新代入式 (2.23) 中并且对 $T$ 进行积分，这里我们同样需要用到之前的积分恒等式 $\int_{-\infty}^{+\infty}dYe^{-Xe^Y+nY}=(n-1)!/X^n$，最终的结果为：

$$\Delta^{(d)}=\frac{k^3}{96\pi}\int_0^{+\infty}dt_d\int_{t_d}^\infty dr\frac{e^{-r}\cos(kt_d)}{r^4\mathcal{I}(t_d,r)^2}\times\frac{j_2(kr)}{k^2r^2}G(t_d,r)G(-t_d,r) \tag{3.38}$$

## 4 数值计算结果

由于在式 (3.28) 和 (3.38) 中仅仅剩下两个积分式不能够直接简单计算的，因此我们在这一小节中利用数值方法进行求解。在图 3-5 中我们给出了单一 Bubble 和双生 Bubble 情形的

引力波谱 $\Delta^{(s)}$ 和 $\Delta^{(d)}$ 以及两者之和 $\Delta = \Delta^{(s)} + \Delta^{(d)}$。由图可知，两者在低频波段和高频波段的行为如下：

$$\Delta^{(s)} \propto \begin{cases} k^3 & (k/\beta \lesssim 1) \\ k^{-1} & (1 \lesssim k/\beta) \end{cases} \tag{4.1}$$

$$\Delta^{(d)} \propto \begin{cases} k^3 & (k/\beta \lesssim 1) \\ k^{-1} & (1 \lesssim k/\beta \lesssim 10) \\ k^{-2} & (10 \lesssim k/\beta) \end{cases} \tag{4.2}$$

由于 $\Delta^{(s)}$ 在所有频段的贡献都大于 $\Delta^{(d)}$ 的贡献因此两者之和的行为大致如下：

$$\Delta \propto \begin{cases} k^3 & (k/\beta \lesssim 1) \\ k^{-1} & (1 \lesssim k/\beta) \end{cases} \tag{4.3}$$

因此文献【36】中给出的高频波段的引力波能量谱的行为与我们的计算相一致。注意到在上面几式中我们已经将 $\beta$ 显式写出。这里我们给出一个谱的拟合公式如下：

$$\Delta = \frac{\Delta_{\text{peak}}}{c_l \left(\frac{f}{f_{\text{peak}}}\right)^{-3} + (1 - c_l - c_h)\left(\frac{f}{f_{\text{peak}}}\right)^{-1} + c_h \left(\frac{f}{f_{\text{peak}}}\right)} \tag{4.4}$$

这里 $\Delta_{\text{peak}} = 0.043$, $f_{\text{peak}}/\beta = 1.24/2\pi \simeq 0.20$ 同时 $(c_l, c_h) = (0.064, 0.48)$。这里的 “$l$” 和 “$h$” 分别表示低频和高频，同时我们还要注意到 $f/f_{\text{peak}} = k/k_{\text{peak}}$。这个拟合公式和精确的谱有 8% 的误差。当前宇宙的谱只需要将式 (4.4) 代入式 (2.26) 即可，其中现在的 $f_{\text{peak}}$ 由式 (2.25) 给出。

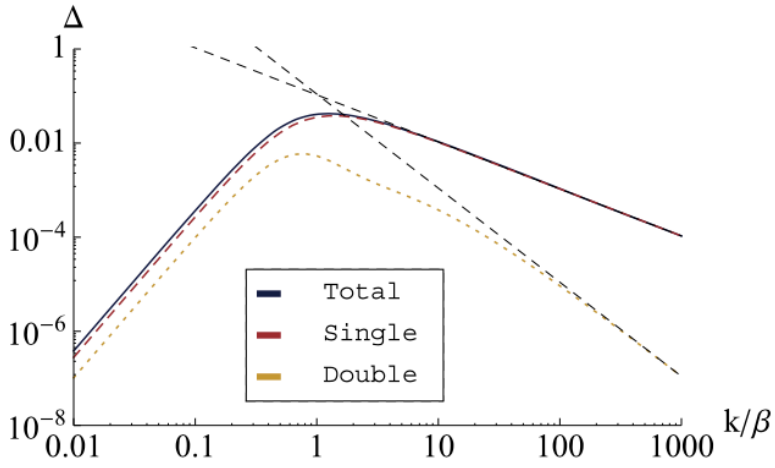


图 4-1　引力波谱示意图。其中 $\Delta$ 用蓝线绘出，$\Delta^{(s)}$ 和 $\Delta^{(d)}$ 分别由红线和黄线绘出。黑线是正比于 $k^{-1}$ 和 $k^{-2}$ 的辅助线。

## 5 非光速情况

虽然在之前的讨论中我们都认为 Bubble 壁以光速运动，但是实际上我们很容易将所有计算的结果推广到 Bubble 壁以任意速度 $v$ 运动的情形。我们只需要将 $r_\bullet \to r_\bullet/v$ 以及 $k \to vk$ 我们就可以重复以上的计算得到结果。最后的结果是我们只需要将能动张量的两点关联函数改写如下：

$$\Pi(t_x, t_y, k) \to v^3 \Pi(t_x, t_y, vk) \tag{5.1}$$

这意味着在 $v \neq c$ 的情况下的关联函数可以如下表示：$\Pi = \Pi_v(t_x, t_y, k) = v^3 \Pi_c(t_x, t_y, vk)$。这里的 $\Pi_v$ 和 $\Pi_c$ 分别是 $v \neq c$ 以及 $v = c$ 情况下的关联函数。因此我们可以得到：

$$\Delta = \Delta^{(s)} + \Delta^{(d)} \tag{5.2}$$

其中

$$\Delta^{(s)} = \frac{v^3 k^3}{12\pi} \int_0^{+\infty} \int_{r_d}^{+\infty} \frac{e^{-r/2} \cos(k t_d)}{r^3 \mathcal{I}(t_d, r)} \left[ j_0(vkr) F_0 + \frac{j_1(vkr)}{vkr} F_1 + \frac{j_2(vkr)}{v^2 k^2 r^2} F_2 \right] \tag{5.3}$$

$$\Delta^{(d)} = \frac{v^3 k^3}{96\pi} \int_0^{+\infty} dt_d \int_{t_d}^{\infty} dr \frac{e^{-r} \cos(k t_d)}{r^4 \mathcal{I}(t_d, r)^2} \times \frac{j_2 v(kr)}{v^2 k^2 r^2} G(t_d, r) G(-t_d, r) \tag{5.4}$$

注意到以上的式子都已经用 $\beta$ 归一化。

就如同我们之前讨论的情况一样，到此为止已经很难继续进行解析的分析了，因此我们采用数值模拟的方法进行计算。图 5-1 中给出了在 $v = 1, 0.1, 0.01$ 情况下的 $\Delta$ 随频率变化的曲线图。单一 Bubble 和双生 Bubble 的贡献同样在图中给出。从图中我们可以看出 $\Delta^{(d)}$ 只有在 $v = c$ 的情况下才满足 $\Delta^{(d)} \propto k^{-2}$，在其他情况下 $\Delta^{(s)}$ 和 $\Delta^{(d)}$ 都分别在低频和高频情况下正比于 $k^3$ 以及 $k^{-1}$。我们可以用如下的泰勒展开来理解这样的行为：

$$\frac{\Delta^{(d)}}{v^3} = \left( \frac{\Delta^{(d)}}{v^3} \right)^{(0)} + \left( 1 - \frac{v}{c} \right) \left( \frac{\Delta^{(d)}}{v^3} \right)^{(1)} + \ldots \tag{5.5}$$

这里我们可以看到当 $v = c$ 的时候除了第一项其他项全都为零。一阶项由下式给出：

$$\left( \frac{\Delta^{(d)}}{v^3} \right)^{(1)} = \frac{k^3}{96\pi} \int_0^{\infty} dt_d \int_{t_d}^{\infty} \frac{e^{-r} \cos(k t_d)}{r^4 \mathcal{I}(t_d, r)^2} \times \frac{j_3(kr)}{k^2 r^2} G(t_d, r) G(-t_d, r) \tag{5.6}$$

它的行为在图 5-2 中给出，我们可以看出在高频波段 $\Delta$ 满足 $k^{-1}$ 的正比关系。正是这样才导致在 $v \neq c$ 的情况下引力波谱的行为如图 4-1 中给出的一样在高频波段满足 $\Delta \propto k^{-1}$。我们的结果与文献【36】中给出的定性行为相同，定量结果的差别也小于 2 倍。

最后我们给出引力波能谱的峰值对应的频率和峰值本身大小的估计公式。Bubble 壁运动速度和能谱峰值以及能谱峰值频率的关系在图 5-3，图 5-4 中用蓝线已经给出，红线所描述的拟合公式如下：

$$\frac{f_{\text{peak}}}{\beta} = \frac{0.35}{1 + 0.069v + 0.69v^4} \tag{5.7}$$

$$\Delta_{\text{peak}} = \frac{0.48 v^3}{1 + 5.3v^2 + 5.0v^4} \tag{5.8}$$

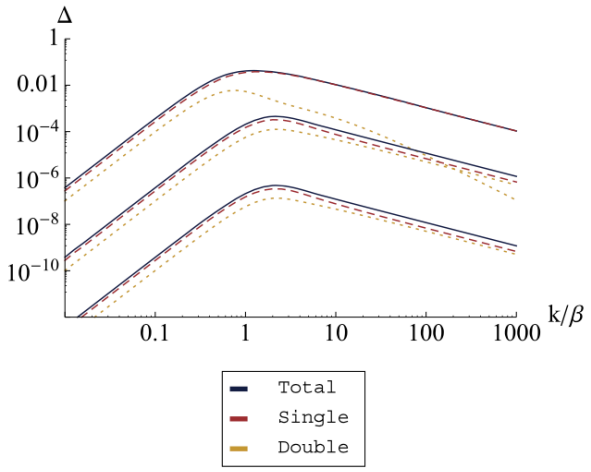


图 5-1　从上到下分别画出了 $v = 1, 0.1, 0.01$ 情况下的 $\Delta$(蓝线)。红线和黄线分别对应单一 Bubble$\Delta^{(s)}$ 和双生 Bubble$\Delta^{(d)}$ 的贡献。

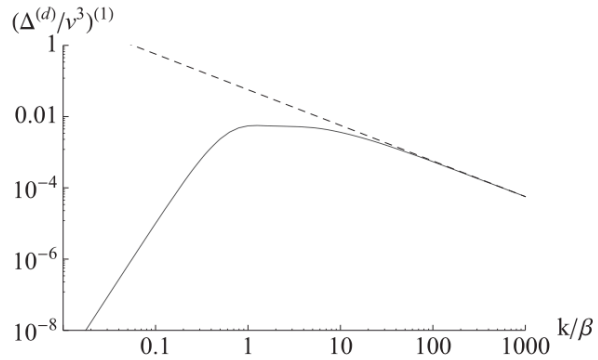


图 5-2　峰值频率 $f_{\text{peak}/\beta}$ 作为 Bubble 壁的运动速度 $v$ 的函数。蓝线是式 (5.3)(5.4) 通过数值计算的结果，红线是式 (5.) 给出的拟合结果

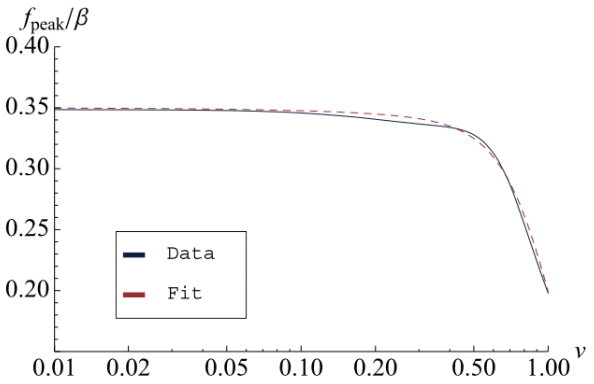


图 5-3　峰值频率 $f_{\text{peak}}/\beta$ 作为 Bubble 壁运动速度 $v$ 的函数。蓝线为式 (5.3)(5.4) 数值计算的结果，红线对应式 (5.7) 的拟合公式。

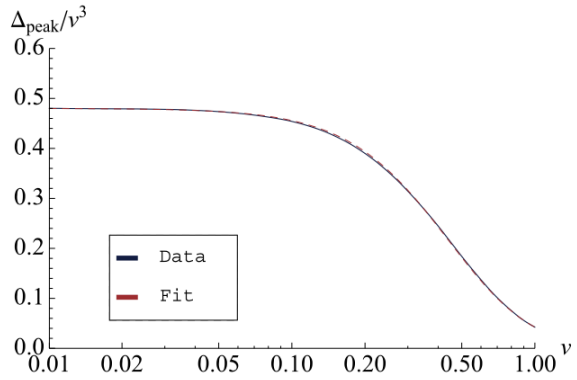


图 5-4　$\Delta_{\text{peak}}/v^3$ 作为 $v$ 的函数。蓝线为式 (5.3)(5.4) 数值计算的结果，红线对应式 (5.8) 的拟合公式。

这两个拟合公式相对计算得到的谱的误差分别在 5% 和 3% 之内。目前和峰值频率和波谱峰值由之前已经给出的式 (2.25) 和 (2.26) 式给出，我们这里为了方便再次给出：

$$f = f_*\left(\frac{a_*}{a_0}\right) = 1.65\times 10^{-5}\text{Hz}\left(\frac{f_*}{\beta}\right)\left(\frac{\beta}{H_*}\right)\left(\frac{T_*}{100\text{GeV}}\right)\left(\frac{g_*}{100}\right)^{1/6} \tag{5.9}$$

$$\Omega_{GW}h^2 = 1.67\times 10^{-5}\kappa^2\Delta\left(\frac{\beta}{H_*}\right)^{-2}\left(\frac{\alpha}{1+\alpha}\right)^2\left(\frac{g_*}{100}\right)^{-1/3} \tag{5.10}$$

这里的 $H_\star, T_\star$ 分别是在相变发生时的哈勃常数以及宇宙的温度。$g_\star$ 是温度为 $T_\star$ 时的相对论性的自由度，$\kappa$ 为等式 (2.2) 中定义的效率，$\alpha, \beta$ 分别为 (2.21) 式定义的释放出来能量密度和辐射的能量密度之比以及 (2.4) 式中给出的与凝结率相关的参数。

## 6　讨论以及结论

在这篇论文中，我们得到了在薄壁近似以及包络近似下的由宇宙学一阶相变过程中 Bubble 碰撞产生的引力波谱的解析表达式。关键在于我们仅仅需要知道能动张量的两点关联函数 $\langle T(x)T(y)\rangle$ 就可以具体计算能谱，而这个两点关联函数的具体解析表达式已经在文中给出。作为一个结论，我们发现单一 Bubble 情形对两点关联函数的贡献是最大的，除此之外，在高频波段引力波的能量谱服从 $\Delta \propto f^{-1}$ 的规律。另外我们也在文中给出了具体的谱拟合公式，可以参考式 (4.4) 以及 (5.7)-(5.10)。

我们所做的分析的关键假设为薄壁近似，这个近似让我们的分析大大简化。因为薄壁近似的保证我们可以将对两点关联的贡献分类为单一 Bubble 和双生 Bubble 情形再具体分析计算。因此事实上我们有可能在保证薄壁近似的前提下分析更多一般的模型。比如我们完全有可能考虑更加一般的 Bubble 凝结率以及将宇宙膨胀具体考虑在计算之内。除此之外，我们也可以在抛弃包络近似的前提下尝试重复所有计算。我们将这些可能的拓展留给未来的研究。

**附录 A：单个 Bubble 情况的具体计算细节**

在这个附录中我们将会给出单一 Bubble 情况下引力波谱的具体计算过程。我们的目的是为了计算得到式 (3.28)，我们要计算的式为：

$$\Delta(k/\beta,v)=\frac{3}{8\pi G}\frac{\beta^2\rho_{tot}}{\kappa^2\rho_0^2}\Omega_{GW}=\frac{3}{4\pi^2}\frac{\beta^2k^3}{\kappa^2\rho_0^2}\int_{t_{start}}^{t_{end}}dt_x\int_{t_{start}}^{t_{end}}dt_y\cos\Big[k(t_x-t_y)\Big]\Pi(t_x,t_y,k) \tag{A1}$$

下面我们不失一般性地取 $\beta=1$。$\Pi$ 由下式给出：

$$\Pi(t_x,t_y,k)=K_{ij,kl}(\boldsymbol{k})K_{ij,mn}(\boldsymbol{k})\int d^3re^{i\boldsymbol{k}\cdot\boldsymbol{r}}\langle T_{kl}T_{mn}\rangle(t_x,t_y,\boldsymbol{r}) \tag{A2}$$

这里的 $K_{ij,kl}$ 是 (2.8) 式给出的投影算子。单一 Bubble 情形对于两点关联函数贡献可以被分解如下：

$$\langle T_{kl}T_{mn}\rangle^{(s)}(t_x,t_y,\boldsymbol{r})=P(t_x,t_y,r)\int_{-\infty}^{t_{xy}}dt_n\Gamma(t_n)\mathcal{T}^{(s)}_{ij,kl}(t,t_x,t_y,\boldsymbol{r}) \tag{A3}$$

这里的 $\mathcal{T}^{(s)}_{ij,kl}$ 是在 $t_n$ 时刻凝结的 Bubble 壁的 $T_{ij}(x)T_{kl}(y)$ 的值。这个式子可以计算如下：

$$\mathcal{T}^{(s)}_{ij,kl}=\left(\frac{4\pi}{3}r_x(t_n)^3\cdot\kappa\rho_0\cdot\frac{1}{4\pi r_x(t_n)^2\ell_B}\right)\times\left(\frac{4\pi}{3}r_y(t_n)^3\cdot\kappa\rho_0\cdot\frac{1}{4\pi r_y(t_n)^2\ell_B}\right)\times\int_{R_{xy}}d^3z\Big(N_x\Big)_{ijkl} \tag{A4}$$

这里的 $(N_\times)_{ijkl}\equiv(n_{x\times})_i(n_{x\times})_j(n_{y\times})_k(n_{y\times})_l$。这里 $R_{xy}\equiv\delta V_{xy}\cap\Sigma_{t_n}$ 为图 3-4 中的红色菱形区域绕着 $\boldsymbol{r}$ 旋转一周形成的环形结构。下面为了方便我们将 $r_xt_n,r_yt_n$ 中的参数 $t_n$ 省略。下面我们将投影算子作用到两点关联函数上并且注意到图 3-4 中菱形区域的面积可以表示为 $l_B^2/\sin(\theta_x-\theta_y)$ 就可以得到如下结果:

$$K_{ij,kl}(\boldsymbol{k})K_{ij,mn}(\boldsymbol{k})\langle T_{kl}T_{mn}\rangle^{(s)}(t_x,t_y,\boldsymbol{r})=\left(\frac{\kappa\rho_0}{3}\right)^2P(t_x,t_y,\boldsymbol{r})\int_{-\infty}^{t_{xy}}dt_n\int d\phi\Gamma(t_n)\frac{r_x^2r_y^2}{r}K_{kl,mn}(N_\times)_{klmn} \tag{A5}$$

这里我们用到了图 3-4 中存在的几个几何关系 $r_xs_{x\times}=r_ys_{y\times}(=r_\perp)$,$-r_xc_{c\times}+r_yc_{y\times}=r$ 以及 $K_{ij,kl}K_{ij,mn}=K_{kl,mn}$。同时我们要注意到 $\phi=\phi_{x\times}=\phi_{y\times}$ 式绕着 $\boldsymbol{r}$ 的方位角。因为在这个系统中除了 $\boldsymbol{r}$ 并不存在其他特殊的方向，因此两点关联函数 $\langle T_{ij}T_{kl}\rangle$ 只可能有如下的项：

$$\begin{aligned}\langle T_{ij}T_{kl}\rangle^{(s)}=&\,a_1\delta_{ij}\delta_{kl}+a_2\frac{1}{2}(\delta_{ik}\delta_{jl}+\delta_{il}\delta_{jk})+b_1\delta_{ij}\boldsymbol{r}_k\boldsymbol{r}_l+b_2\delta_{kl}\boldsymbol{r}_i\boldsymbol{r}_j\\&+b_3\frac{1}{4}(\delta_{ik}\boldsymbol{r}_j\boldsymbol{r}_l+\delta_{il}\boldsymbol{r}_j\boldsymbol{r}_k+\delta_{jk}\boldsymbol{r}_i\boldsymbol{r}_l+\delta_{jl}\boldsymbol{r}_i\boldsymbol{r}_k)\\&+c_1\boldsymbol{r}_i\boldsymbol{r}_j\boldsymbol{r}_k\boldsymbol{r}_l\end{aligned} \tag{A6}$$

这里给出的 $a,b,c$ 是我们需要确定的几个参数。在做了投影操作后仅仅有如下几项贡献非零：

$$K_{ij,kl}(\boldsymbol{k})K_{ij,mn}(\boldsymbol{k})\langle T_{kl}T_{mn}\rangle^{(s)}=2a_2+(1-c_{rk}^2)b_3+\frac{1}{2}(1-c_{rk}^2)^2c_1 \tag{A7}$$

这里的 $c_{rk} \equiv \hat{r} \cdot \hat{k}$。参数 $a, b, c$ 可以通过指定 $\boldsymbol{r}$ 方向为 $\hat{z}$ 方向来计算得到：

$$\langle T_{xx}T_{xx}\rangle^{(s)} = a_1 + a_2 \quad \langle T_{xy}T_{xy}\rangle^{(s)} = \frac{1}{2}a_2 \quad \langle T_{xx}T_z\rangle^{(s)} = a_1 + b_1 \quad \langle T_{zz}T_{xx}\rangle^{(s)} = a_1 + b_2$$

$$\langle T_{xz}T_{xz}\rangle^{(s)} = \frac{1}{2}a_2 + \frac{1}{4}b_3 \quad \langle T_{zz}T_{zz}\rangle^{(s)} = a_1 + a_2 + b_1 + b_2 + b_3 + c_1 \tag{A8}$$

于是我们可以得到如下结果：

$$\begin{aligned} a_2 &= 2\langle T_{xy}T_{xy}\rangle^{(s)} \\ b_3 &= 4\left(\langle T_{xz}T_{xz}\rangle^{(s)} - \langle T_{xy}T_{xy}\rangle^{(s)}\right) \\ c_1 &= \langle T_{xx}T_{xx}\rangle^{(s)} - \left(\langle T_{xx}T_{zz}\rangle^{(s)} + \langle T_{zz}T_{xx}\rangle^{(s)}\right) - 4\langle T_{xz}T_{xz}\rangle^{(s)} + \langle T_{zz}T_{zz}\rangle^{(s)} \end{aligned} \tag{A9}$$

因此我们可以将投影后的两点关联函数写成如下形式：

$$\begin{aligned} &K_{ij,kl}(\boldsymbol{k})K_{ij,mn}(\boldsymbol{k})\langle T_{kl}T_{mn}\rangle^{(s)}(t_x, t_y, \boldsymbol{r}) \\ &= \left(\frac{\kappa\rho_0}{3}\right)^2 P(t_x, t_y, r)\int_{-\infty}^{t_{xy}} dt_n \int d\phi \frac{r_x^2 r_y^2}{r} \times \Big[4N_{xy,xy} + 4(1 - c_{rk}^2(N_{xz,xz} + N_{xy,xy})) \\ &+ \frac{1}{2}(1 - c_{rk}^2) \times (N_{xx,xx} - (N_{xx,zz} + N_{zz,xx}) - 4N_{xz,xz} + N_{zz,zz})\Big] \end{aligned} \tag{A10}$$

其中

$$F_0' = s_{x\times}^2 s_{y\times}^2 \tag{A11}$$

$$F_1' = 8s_{x\times}c_{x\times}s_{y\times}c_{y\times} - 2s_{x\times}^2 s_{y\times}^2 \tag{A12}$$

$$F_2' = 3s_{x\times}^2 s_{y\times}^2 - 4\left(s_{x\times}^2 c_{y\times}^2 + c_{x\times}^2 s_{y\times}^2\right) - 16s_{x\times}c_{x\times}s_{y\times}c_{y\times} + 8c_{x\times}^2 c_{y\times}^2 \tag{A13}$$

利用 $r_x s_{x\times} = r_y s_{y\times}$，我们可以将让根号下的仅仅出现 $s_x^2, s_y^2$ 而不出现 $s_x, s_y$。

$$\begin{aligned} &K_{ij,kl}(\boldsymbol{k})K_{ij,mn}(\boldsymbol{k})\langle T_{kl}T_{mn}\rangle^{(s)}(t_x, t_y, \boldsymbol{r}) = \\ &\qquad \frac{2\pi}{9}\kappa^2\rho_0^2 P(t_x, t_y, r)\int_{-\infty}^{t_{xy}} \frac{\Gamma(t_n)}{r}\left[\frac{1}{2}F_0'' + \frac{1}{4}(1 - c_{rk}^2)F_1'' + \frac{1}{16}(1 - c_{rk}^2)F_2''\right]dt_n \end{aligned} \tag{A14}$$

其中

$$F_0'' = r_x^2 r_y^2 s_{x\times}^2 s_{y\times}^2 \tag{A15}$$

$$F_1'' = r_x r_y\left[4c_{x\times}c_{y\times}(r_x^2 s_{x\times}^2 + r_y^2 s_{y\times}^2) - 2r_x r_y s_{x\times}^2 s_{y\times}^2\right] \tag{A16}$$

$$F_2'' = r_x r_y\left[r_x r_y(19c_{x\times}^2 c_{y\times}^2 - 7(c_{x\times}^2 + c_{y\times}^2) + 3) - 8c_{x\times}c_{y\times}(r_x^2 s_{x\times}^2 + r_y^2 s_{y\times}^2)\right] \tag{A17}$$

这样就可以让我们的被积函数中不会出现由 $s_{x\times} = \sqrt{1 - c_x^2}$ 带来的根号。

现在我们将被积函数中的 Bubble 凝结时间 $t_n$ 这一时间参数由 $t_n$ 转换为 $t_T \equiv t_n - T$。

这里我们注意到对由于 $t_{xy} = T - r/2$ 因此 $t_T$ 的积分是从 $-\infty$ 到 $-r/2$ 的。同时我们注意到 $F_0'', F_1''$ 以及 $F_2''$ 仅仅是 $t_T$ 的多项式并且 $\Gamma(t_n)$ 可以写成 $\Gamma(t_n)$。因此我们可以再次将以上式子改写如下：

$$K_{ij,kl}(\boldsymbol{k})K_{ij,mn}(\boldsymbol{k})\langle T_{kl}T_{mn}\rangle^{(s)}(t_x,t_y,\boldsymbol{r}) = \frac{2\pi}{9}\kappa^2\rho_0^2 P(t_x,t_y,r)^{\Gamma}(T)\frac{e^{-r/2}}{r^5}\left[\frac{1}{2}F_0 + \frac{1}{4}(1-c_{rk}^2)F_1 + \frac{1}{16}(1-c_{rk}^2)F_2\right]dt_n \tag{A18}$$

其中

$$F_0 = 2(r^2 - t_d^2)^2(r^2 + 6r + 12) \tag{A19}$$

$$F_1 = 2(r^2 - t_d^2)\left[-r^2(r^3 + 4r^2 + 12r + 24) + t_d^2(r^3 + 12r^2 + 60r + 120)\right] \tag{A20}$$

$$F_2 = \frac{1}{2}\Big[r^4(r^4 + 4r^3 + 20r^2 + 72r + 144) - 2t_d^2r^2(r^4 + 12r^3 + 84r^2 + 360r + 720) + t_d^4(r^4 + 20r^3 + 180r^2 + 840r = 1680)\Big] \tag{A21}$$

在式 (A2) 中，对于 $\boldsymbol{r}$ 和 $\boldsymbol{k}$ 之间的夹角的积分是很容易计算的，因为被积函数对于这个角度的依赖关系仅仅是通过 $c_{rk}$ 体现的。我们注意到有以下的恒等式：

$$\int_{-1}^{+1} dce^{icx} = 2j_0(x) \quad \int_{-1}^{+1} dce^{icx}(1-c^2) = \frac{4j_1(x)}{x} \quad \int_{-1}^{+1} e^{icx}(1-c^2)^2 = \frac{16j_2(x)}{x^2} \tag{A22}$$

其中 $j_i$ 是球贝塞尔函数

$$\begin{aligned} j_0(x) &= \frac{\sin x}{x} \\ j_1(x) &= \frac{\sin x - x\cos x}{x^2} \\ j_2(x) &= \frac{(3-x^2)\sin x - 3x\cos x}{x^3} \\ j_3(x) &= \frac{(15-6x^2)\sin x - (15x - x^3)\cos x}{x^4} \end{aligned} \tag{A23}$$

因此我们有：

$$\Pi^{(s)}(t_x,t_y,k) = \frac{4\pi^2}{9}\kappa^2\rho_0^2\Gamma(T)\int_0^{\infty} dr\frac{e^{-r/2}}{r^3}P(t_x,t_y,r)\times\left[j_0(kr)F_0 + \frac{j_1(kr)}{kr}F_1 + \frac{j_2(kr)}{k^2r^2}F_2\right] \tag{A24}$$

最后我们考虑式 (A1) 中对时间 $T \equiv (t_1+t_2)/2$ 的积分。由于 $P(x,y)$ 如下：

$$P(x,y) = e^{-8\pi\Gamma(T)\mathcal{I}(t_d,r)} \tag{A25}$$

$\Pi^{(s)}(t_x,t_y,k)$ 对 $T$ 的依赖关系仅仅在 $\Gamma(T)e^{-8\pi\Gamma(T)\mathcal{I}(t_d,r)}$ 这一因子中出现。通过利用恒等关系：$\int_{-\infty}^{+\infty} dYe^{-Xe^Y+nY} = (n-1)!/X^n$，对 $T$ 的积分可以解析得到。最后我们可以得到如下

结果：

$$\Delta^{(s)} = \frac{k^3}{12\pi}\int_0^{+\infty}\int_{r_d}^{+\infty}\frac{e^{-r/2}\cos(kt_d)}{r^3\mathcal{I}(t_d,r)}\left[j_0(kr)F_0 + \frac{j_1(kr)}{kr}F_1 + \frac{j_2(kr)}{k^2r^2}F_2\right] \tag{A26}$$

**附录 B：对于“球对称”的评述**

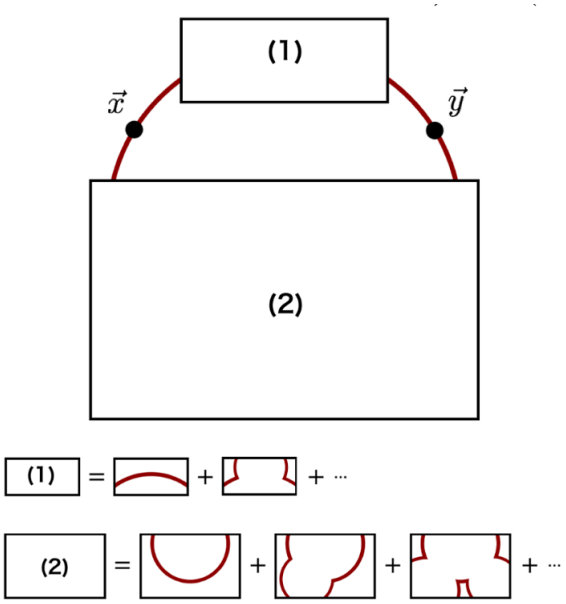


图 6-1　对于为什么单一 Bubble 下的球对称不会影响我们的计算。在这一幅图中我们设置 $t_x = t_y$。我们要求 Bubble 壁在传播到 $\boldsymbol{x}, \boldsymbol{y}$ 之前是没有经过碰撞的，但是 Bubble 壁的其他部分是可以与其他 Bubble 发生碰撞的。这样就通过 Bubble 碰撞将单一 Bubble 情形下的球对称破坏。

众所周知完美的球对称的物体是不会辐射引力波的。在这个附录中我们将解释所谓“球对称”的考虑不会否定我们之前的计算，特别是对于单一 Bubble 情形的讨论。

在我们的推导中非常明显地可以看出，特别是对于单一 Bubble 情况，我们的计算并不是在两个完整的球面上计算 $\boldsymbol{x}$ 和 $\boldsymbol{y}$ 的贡献。反而我们首先固定这两个我们考察的时空点然后再具体分析那些在一个点凝结的 Bubble 对 $\boldsymbol{x}$ 和 $\boldsymbol{y}$ 两点的能动张量的贡献。在这样的过程中我们将 $x, y$ 两点固定时就自动将球对称性的破缺考虑在内了，因为那些传播向我们的考察点的 Bubble 壁被要求是在经过这两个点之前还没有经过碰撞的，但是并没有任何条件要求这个 Bubble 的其他部分没有发生碰撞。

我们在图。中给出了具体的解释。假设我们固定 $x$ 和 $y$，并且考虑 $t_x = t_y$ 的情形。那么在这个考察时间点时在区域 (1) 和 (2) 内的 Bubble 壁仍然处于未碰撞状态并且是形成了一个完整球体的一部分 (图中等式的左边)，但是在其他情况下 (不同的 $t_x, t_y$ 取值)，它们事实上已经与其他 Bubble 产生了碰撞 (图中等式的右边)。另一方面，Bubble 壁的组成部分在传到 $\boldsymbol{x}, \boldsymbol{y}$ 两点前必须保证在我们的考察时间之前没有发生碰撞。因此我们的计算与通常意义

上的“球对称”没有什么关联，并且由于 Bubble 碰撞而自动将球对称破坏。

# 参考文献原文

PHYSICAL REVIEW D **95,** 024009 (2017)

# Gravitational waves from bubble collisions: An analytic derivation

Ryusuke Jinno and Masahiro Takimoto
*Theory Center, High Energy Accelerator Research Organization (KEK), 1-1 Oho, Tsukuba, Ibaraki 305-0801, Japan*
(Received 28 July 2016; published 5 January 2017)

We consider gravitational wave production by bubble collisions during a cosmological first-order phase transition. In the literature, such spectra have been estimated by simulating the bubble dynamics, under so-called thin-wall and envelope approximations in a flat background metric. However, we show that, within these assumptions, the gravitational wave spectrum can be estimated in an analytic way. Our estimation is based on the observation that the two-point correlator of the energy-momentum tensor $\langle T(x)T(y)\rangle$ can be expressed analytically under these assumptions. Though the final expressions for the spectrum contain a few integrations that cannot be calculated explicitly, we can easily estimate it numerically. As a result, it is found that the most of the contributions to the spectrum come from single-bubble contribution to the correlator, and in addition the fall-off of the spectrum at high frequencies is found to be proportional to $f^{-1}$. We also provide fitting formulas for the spectrum.

DOI: 10.1103/PhysRevD.95.024009

## I. INTRODUCTION

Gravitational waves (GWs) are one of the promising tools to probe the early universe. They provide a unique way to search for inflationary quantum fluctuations [1], preheating [2], topological defects [3,4], and cosmic phase transitions (PTs) [5,6]. Especially, first-order PTs in the early universe have been attractive to us because of their relation to high-energy physics beyond the standard model (SM), and in fact various extensions of the SM have been shown to predict first-order PTs with a large amount of GWs [7–21]. On the observational side, ground-based GW experiments like KAGRA [22], VIRGO [23] and Advanced LIGO [24] are now in operation, and space interferometers such as eLISA [25], BBO [26] and DECIGO [27] have been proposed. Given that there is a growing possibility of their detecting GWs from cosmological sources in the near future, it would be worth reconsidering the theoretical predictions of GWs from first-order PTs.

First-order PTs proceed via the nucleation of bubbles, their expansion, collision and thermalization into light particles, and GWs are produced during this process.[1] In the transition process, some of the released energy goes into heating up the plasma, while the rest is carried by the scalar field configuration (bubble wall) and/or the bulk motion of the surrounding fluid. Gravitational wave production by such localized structure of energy around the walls has been calculated by numerical simulations in the literature with so-called thin-wall and envelope approximations [29–32].[2] It has been shown that these approximations are valid especially when the energy of bubbles is dominated by the scalar field configuration [29,36], and the latest result along this approach is found in Ref. [37]. Analytic approaches have also been taken with some ansatz for correlator functions [38,39].

In this paper, we take an approach based on the evaluation of the correlation function of the energy-momentum tensor $\langle T(x)T(y)\rangle$ [38], which is the only ingredient to obtain the spectrum. We point out that, under thin-wall and envelope approximations and in a flat background, this two-point correlator has a rather simple analytic expression and, as a result, the GW spectrum can also be expressed analytically. Though the final expression for the spectrum contains two remaining integrations, they can easily be estimated numerically. Our approach is not only free from statistical errors inherent to numerical simulations, but also enables us to specify the most effective bubble-wall configuration to the GW spectrum. At the current stage, our results are most relevant to strong phase transitions like near-vacuum ones, since the neglected effects such as the finite width of the bubble walls and/or the localized structure of the energy-momentum tensor remaining after collisions can be important when the scalar field is strongly coupled to the thermal plasma [33–35].[3] However, our method is extendable to the calculations without the envelope approximation [43], and such studies would be important in understanding how the localized structure after bubble collisions sources GWs.

The organization of the paper is as follows. In Sec. II we first make clear our assumptions in estimating the GW spectrum, i.e. thin-wall and envelope approximations, and

[1]See Ref. [28] for the latest understanding on various GW sources from first-order PTs.

[2]It is important to go beyond these approximations, especially when the bulk motion of the fluid dominates the released energy. In fact, it has been pointed out that the bulk motion can be a long-lasting GW source as sound waves [33–35].

[3]In addition, turbulent effects can contribute sizably to the GW spectrum [32,40–42].

 

then introduce basic ingredients such as the evolution equation and power spectrum of GWs. In Sec. III we present analytic expressions for the GW spectrum. Since two integrations cannot be performed explicitly, we evaluate them numerically in Sec. IV. We generalize our result to finite velocity case in Sec. V, and finally summarize in Sec. VI.

## II. BASIC INGREDIENTS

In this section we summarize basic ingredients for the calculation of the GW spectrum. We first make clear the assumption and approximations used in the paper. We also explain the GW power spectrum around the time of sourcing from bubble collisions, and then show how to obtain the present spectrum.

### A. Assumptions and approximations

#### 1. Thin wall and envelope approximation

In this subsection, we introduce the key assumptions to characterize the energy momentum tensor around the bubble wall, namely thin-wall and envelope approximations.

First, we introduce the thin-wall approximation, where all the energy of the bubble is assumed to be concentrated on the bubble wall with an infinitesimal width. We introduce the infinitesimal wall width $l_B$ for computational simplicity. The energy momentum tensor $T^B$ of the uncollided wall of a single bubble nucleated at $x_N \equiv (t_N, \vec{x}_N)$ can be written as

$$T^B_{ij}(x) = \rho(x)\widehat{(x-x_N)}_i\widehat{(x-x_N)}_j, \tag{1}$$

with

$$\rho(x) = \begin{cases} \frac{4\pi}{3} r_B(t)^3 \frac{\kappa\rho_0}{4\pi r_B(t)^2 l_B} & r_B(t) < |\vec{x}-\vec{x}_N| < r'_B(t) \\ 0 & \text{otherwise} \end{cases} \tag{2}$$

and

$$r_B(t) = v(t-t_N), \qquad r'_B(t) = r_B(t) + l_B. \tag{3}$$

Here $x \equiv (t, \vec{x})$, the hat on the vector $\hat{\bullet}$ indicates the unit vector in the direction of $\vec{\bullet}$, $v$ is the bubble wall velocity, and $\rho_0$ represents the energy density released by the transition.[4] Also, $\kappa$ indicates the efficiency factor, which determines the fraction of the released energy density which is transformed into the energy density localized around the wall[5] [32]. In addition, the Latin indices run over 1,2,3 throughout the paper. Second, we assume that the energy momentum tensor of the bubble walls vanishes once they collide with others. In the literature this is called envelope approximation, whose validity in bubble collisions is discussed in e.g. Ref. [29]. See Fig. 1 for a rough sketch of these approximations. These two assumptions make the calculation of the GW spectrum rather simple, as we will see later. Also, we regard the model-dependent quantities $v$, $\rho_0$ and $\kappa$ as free parameters constant in time.

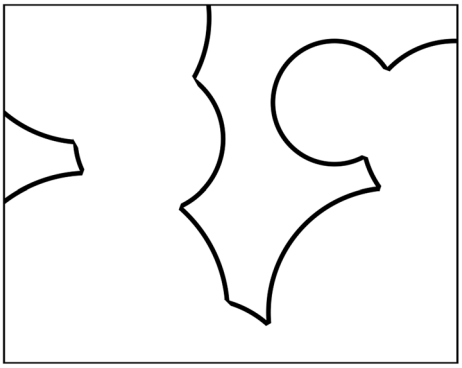

FIG. 1. Rough sketch of how the phase transition looks with the envelope and thin-wall approximations. Collided walls are neglected as a source of GWs, and every spacial point is passed by bubble walls only once.

#### 2. Transition rate

We assume that the bubble nucleation rate per unit time and volume can be written in the following form:

$$\Gamma(t) = \Gamma_* e^{\beta(t-t_*)}, \tag{4}$$

where $t_*$ indicates some fixed time typically around the transition time, $\Gamma_*$ is the nucleation rate at $t = t_*$, and $\beta$ is assumed to be a constant. This parameter $\beta$ is often calculated with the instanton method from underlying models [46,47], and the typical time span of the phase transition is given by $\delta t \sim \beta^{-1}$. We also assume that the phase transition completes in a short period compared to the Hubble time, i.e. $\beta/H \gg 1$, which typically holds for thermal phase transitions [32].

### B. GW power spectrum around the transition time

In the following we express the GW spectrum in terms of the correlator of the energy-momentum tensor, following Ref. [38].

[4]Though the corresponding quantity is latent heat and not energy density in thermal environment, we use the word "energy density" throughout the paper, since GWs from bubble collisions are most relevant to strong phase transitions where the vacuum energy dominates thermal energy.

[5]This corresponds to the energy density of the bulk fluid around the wall when the bubble wall reaches a terminal velocity, while it is the energy density of the wall itself when the scalar field carries most of the energy. In the former case with so-called Jouguet detonation, the efficiency factor is related to the parameter $\alpha$ introduced later [44]. In more general combustion modes, it can be calculated as a function of $\alpha$ and the wall velocity [45].

### 1. Equation of motion and its solution

In this paper we consider GWs sourced by the first order phase transition completed in a short period compared to the Hubble time. In such cases the background metric is well approximated by the Minkowski one. Including tensor perturbations, we write the metric as

$$ds^2 = -dt^2 + (\delta_{ij} + 2h_{ij})dx^i dx^j. \tag{5}$$

The tensor perturbations satisfy the transverse and traceless condition $h_{ii} = \partial_j h_{ij} = 0$ and obey the following evolution equation at the linearized level

$$\ddot{h}_{ij}(t,\vec{k}) + k^2 h_{ij}(t,\vec{k}) = 8\pi G \Pi_{ij}(t,\vec{k}), \tag{6}$$

where $G$ is the Newton constant and $\bullet(t,\vec{k})$ indicates a Fourier mode of the corresponding object with $\vec{k}$ being the wave vector. We take the convention for Fourier transformation to be $\int d^3x e^{i\vec{k}\cdot\vec{x}}$ and $\int d^3k/(2\pi)^3 e^{-i\vec{k}\cdot\vec{x}}$. The source term $\Pi_{ij}$ during the phase transition is given by the transverse and traceless projection of the energy momentum tensor

$$\Pi_{ij}(t,\vec{k}) = K_{ij,kl}(\hat{k}) T_{kl}(t,\vec{k}), \tag{7}$$

with $T_{ij}$ being the energy momentum tensor, and $K_{ij,kl}$ being the projection

$$K_{ij,kl}(\hat{k}) = P_{ik}(\hat{k})P_{jl}(\hat{k}) - \frac{1}{2}P_{ij}(\hat{k})P_{kl}(\hat{k}), \tag{8}$$

$$P_{ij}(\hat{k}) \equiv \delta_{ij} - \hat{k}_i \hat{k}_j. \tag{9}$$

We assume that the source term is effective from $t_{\rm start}$ to $t_{\rm end}$, and we set $t_{\rm start/end} \to \mp\infty$ at the end of the calculation.[6]

The solution of Eq. (6) is formally written in terms of the Green function $G_k$ satisfying $G_k(t,t) = 0$ and $\partial G_k(t,t')/\partial t|_{t=t'} = 1$ as

$$h_{ij}(t,\vec{k}) = 8\pi G \int_{t_{\rm start}}^{t} dt' G_k(t,t')\Pi_{ij}(t',\vec{k}) \qquad t < t_{\rm end}, \tag{10}$$

where $G_k(t,t') = \sin(k(t-t'))/k$. For $t > t_{\rm end}$, matching conditions at $t = t_{\rm end}$ give

$$h_{ij}(t,\vec{k}) = A_{ij}(\vec{k})\sin(k(t-t_{\rm end})) + B_{ij}(\vec{k})\cos(k(t-t_{\rm end})), \tag{11}$$

with coefficients

$$A_{ij}(\vec{k}) = \frac{8\pi G}{k}\int_{t_{\rm start}}^{t_{\rm end}} dt \cos(k(t_{\rm end}-t))\Pi_{ij}(t,\vec{k}), \tag{12}$$

$$B_{ij}(\vec{k}) = \frac{8\pi G}{k}\int_{t_{\rm start}}^{t_{\rm end}} dt \sin(k(t_{\rm end}-t))\Pi_{ij}(t,\vec{k}). \tag{13}$$

### 2. Power spectrum

The energy density of GWs is given by

$$\rho_{\rm GW}(t) = \frac{\langle \dot{h}_{ij}(t,\vec{x})\dot{h}_{ij}(t,\vec{x})\rangle}{8\pi G}, \tag{14}$$

where the angular bracket denotes taking both time average for several oscillation periods and ensemble average. The latter is allowed because GWs from bubble collisions form stochastic background. We often consider the energy density per each logarithmic wave number, normalized by the total energy density of the universe $\rho_{\rm tot}$

$$\Omega_{\rm GW}(t,k) \equiv \frac{1}{\rho_{\rm tot}}\frac{d\rho_{\rm GW}}{d\ln k} = \frac{k^3}{16\pi^3 G\rho_{\rm tot}} P_{\dot{h}}(t,k), \tag{15}$$

where $P_{\dot{h}}$ is the power spectrum of $\dot{h}$

$$\langle \dot{h}_{ij}(t,\vec{k})\dot{h}^*_{ij}(t,\vec{q})\rangle = (2\pi)^3\delta^{(3)}(\vec{k}-\vec{q})P_{\dot{h}}(t,k). \tag{16}$$

The power spectrum $P_{\dot{h}}$ is related to the correlator of the source term $\Pi_{ij}$. Let us define the unequal-time correlator of $\Pi_{ij}$ as

$$\langle \Pi_{ij}(t_x,\vec{k})\Pi^*_{ij}(t_y,\vec{q})\rangle = (2\pi)^3\delta^{(3)}(\vec{k}-\vec{q})\Pi(t_x,t_y,k). \tag{17}$$

Note that the $(2\pi)^3\delta^{(3)}(\vec{k}-\vec{q})$ above appears due to the spacial homogeneity of the system. In terms the original energy-momentum tensor, the correlator $\Pi(t_x,t_y,k)$ is written as

$$\Pi(t_x,t_y,k) = K_{ij,kl}(\hat{k})K_{ij,mn}(\hat{k})\int d^3r e^{i\vec{k}\cdot\vec{r}}\langle T_{kl}T_{mn}\rangle(t_x,t_y,\vec{r}), \tag{18}$$

where

$$\langle T_{kl}T_{mn}\rangle(t_x,t_y,\vec{r}) \equiv \langle T_{kl}(t_x,\vec{x})T_{mn}(t_y,\vec{y})\rangle, \tag{19}$$

with $\vec{r} \equiv \vec{x} - \vec{y}$. The left-hand side (L.H.S.) depends only on $\vec{r}$ because of the spacial homogeneity. Now let us

[6]Since we assume that the transition completes in a short period $\delta t \sim \beta^{-1} \ll H^{-1}$, and GWs are emitted only during this period, this procedure is not expected to affect the result.

consider time $t > t_{\rm end}$. From Eqs. (11), (16) and (17) we have

$$P_{\dot{h}}(t,k) = 32\pi^2 G^2 \int_{t_{\rm start}}^{t_{\rm end}} dt_x \times \int_{t_{\rm start}}^{t_{\rm end}} dt_y \cos(k(t_x - t_y))\Pi(t_x, t_y, k). \quad (20)$$

Though we put the argument $t$ in the L.H.S., the right-hand side (R.H.S.) does not depend on it because there is no source term for $t > t_{\rm end}$ and because we neglect the cosmic expansion. Substituting Eq. (20) into Eq. (15), one finds that $\Omega_{\rm GW}$ is related to $\Pi$ as

$$\Omega_{\rm GW}(t,k) = \frac{2Gk^3}{\pi\rho_{\rm tot}} \int_{t_{\rm start}}^{t_{\rm end}} dt_x \times \int_{t_{\rm start}}^{t_{\rm end}} dt_y \cos(k(t_x - t_y))\Pi(t_x, t_y, k). \quad (21)$$

Now all we have to do is to estimate $\Pi(t_x, t_y, k)$, or the two-point function of the energy momentum tensor $\langle T(x)T(y)\rangle$. As shown later, this correlator $\langle T(x)T(y)\rangle$ can be expressed analytically under the thin-wall and envelope approximations [see Eqs. (50) and (59)].

For later convenience, we rewrite the expression for the GW spectrum as follows. We define the parameter $\alpha$ as

$$\alpha \equiv \frac{\rho_0}{\rho_{\rm rad}}, \qquad \rho_{\rm tot} = \rho_0 + \rho_{\rm rad}, \quad (22)$$

which characterizes the fraction of the released energy density to that of radiation. Here $\rho_{\rm tot}$ and $\rho_{\rm rad}$ are the total and radiation energy density, respectively. Using $\alpha$ thus defined, we have

$$\Omega_{\rm GW}(t,k) = \kappa^2 \left(\frac{H_*}{\beta}\right)^2 \left(\frac{\alpha}{1+\alpha}\right)^2 \Delta(k/\beta, v), \quad (23)$$

where $\Delta$ is given by

$$\Delta(k/\beta, v) = \frac{3}{8\pi G}\frac{\beta^2\rho_{\rm tot}}{\kappa^2\rho_0^2}\Omega_{\rm GW}(t,k) = \frac{3}{4\pi^2}\frac{\beta^2 k^3}{\kappa^2\rho_0^2}\int_{t_{\rm start}}^{t_{\rm end}} dt_x \int_{t_{\rm start}}^{t_{\rm end}} dt_y \cos(k(t_x - t_y))\Pi(t_x, t_y, k). \quad (24)$$

In deriving Eq. (23) we have used the Friedmann equation $H_*^2 = (8\pi G/3)\rho_{\rm tot}$ with $H_*$ being the Hubble parameter at the transition time. Note that the function $\Delta$ depends only on the combination $k/\beta$ and the wall velocity $v$, because the definition (23) factors out $G$, $\kappa$, $\rho_0$ and $\rho_{\rm tot}$ dependence, and because $\Delta$ is a dimensionless quantity.

### C. GW power spectrum at present

After produced, GWs are redshifted during propagation towards the present time. The relation between the scale factor just after the phase transition $a_*$ and at present $a_0$ is given by

$$\frac{a_*}{a_0} = 8.0 \times 10^{-16}\left(\frac{g_*}{100}\right)^{-1}\left(\frac{T_*}{100\ {\rm GeV}}\right)^{-1}, \quad (25)$$

where $T_*$ denotes the temperature just after the phase transition, and $g_*$ indicates the total number of the relativistic degrees of freedom in the thermal bath at temperature $T_*$. The present frequency is obtained by redshifting as

$$f = f_*\left(\frac{a_*}{a_0}\right) = 1.65 \times 10^{-5}\ {\rm Hz}\left(\frac{f_*}{\beta}\right)\left(\frac{\beta}{H_*}\right)\left(\frac{T_*}{100\ {\rm GeV}}\right)\left(\frac{g_*}{100}\right)^{\frac{1}{6}}, \quad (26)$$

and the present GW amplitude is obtained by noticing that GWs are noninteracting radiation as

$$\Omega_{\rm GW}h^2 = 1.67 \times 10^{-5}\left(\frac{g_*}{100}\right)^{-\frac{1}{3}}\Omega_{\rm GW}h^2|_{t=t_{\rm end}} = 1.67 \times 10^{-5}\kappa^2\Delta\left(\frac{\beta}{H_*}\right)^{-2}\left(\frac{\alpha}{1+\alpha}\right)^2\left(\frac{g_*}{100}\right)^{-\frac{1}{3}}. \quad (27)$$

## III. ANALYTIC EXPRESSION

The following sections are mainly devoted to the calculation of $\Delta$ [see Eq. (24)]. We first focus on the case where the wall velocity is luminal, i.e., $v = c$, since the final explanations become relatively simple in this case. Generalization to $v \neq c$ is straightforward and done in Sec. V.

In the expression of the GW spectrum (24), the only nontrivial quantity is the two-point correlator $\Pi(t_x, t_y, \vec{r})$ given by Eq. (18). If we can calculate this quantity, or equivalently the average of the product of the energy-momentum tensor $\langle T_{ij}T_{kl}\rangle(t_x, t_y, \vec{r})$ with given $t_x$, $t_y$ and $\vec{r} = \vec{x} - \vec{y}$, then we obtain the GW spectrum. In the following we show that this is indeed possible. For the energy momentum tensor to be nonzero at $x = (t_x, \vec{x})$ and $y = (t_y, \vec{y})$ with $\vec{x} - \vec{y} = \vec{r}$, the following two conditions are necessary and sufficient:

(i) No bubbles are nucleated inside the past light cones of $x$ and $y$.
(ii) Bubble(s) are nucleated on the past light cones of $x$ and $y$, so that bubble walls are passing through the spacial points $\vec{x}$ at time $t_x$ and $\vec{y}$ at time $t_y$.

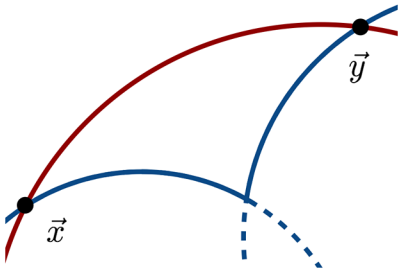


FIG. 2. Schematic picture of single- and double-bubble contributions to the correlator $\langle T(x)T(y)\rangle$. The red line (the one w/o dashed lines) corresponds to the wall of one single bubble, while the blue line (the one w/ dashed lines) corresponds to intersecting two bubble walls. The dashed lines are neglected in the envelope approximation. Note that, though this figure shows $t_x = t_y$ case for simplicity, contributions from $t_x \neq t_y$ exist in the calculation of $\langle T(x)T(y)\rangle$.

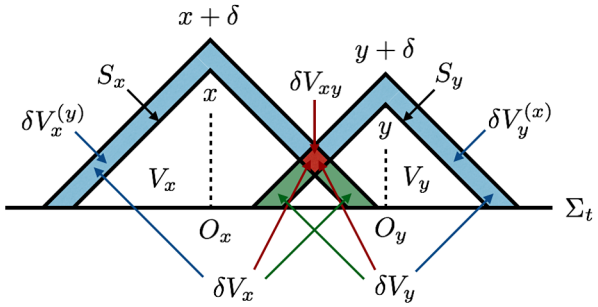


FIG. 3. Notations for quantities on the past light cones of $x$ and $y$.

In order to understand the former condition, notice that any spacial point is passed by bubble walls only once in the envelope approximation (see Fig. 1). Then, if bubble(s) nucleate inside the past light cone of $x$ or $y$, either of the spacial points $\vec{x}$ or $\vec{y}$ is already passed by bubble walls before the evaluation time $t_x$ or $t_y$. This makes it impossible for the energy-momentum tensor to be nonvanishing both at $x$ and $y$, and therefore we need the former condition. On the other hand, the latter condition is necessary for bubble walls to be just passing through $\vec{x}$ and $\vec{y}$ at the evaluation time $t_x$ and $t_y$. There are two possibilities for this condition: these bubble walls belong to one single nucleation point, or to two different nucleation points. We refer to these two as "single-bubble" and "double-bubble" contributions, respectively. Figure 2 shows a schematic picture of these two contributions to the correlator $\langle T(x)T(y)\rangle$. Here one may wonder why we consider the single-bubble contribution, since it is well known that a spherical object do not radiate GWs. The answer is that the single-bubble contribution takes into account the breaking of the original spherical symmetry of a bubble by collisions with others: see Appendix B on this point.

In the following discussion, we first make our notation clear. Then, after discussing the condition for no bubble nucleation inside the past light cones, we consider single- and double-bubble contributions separately. The final expressions are Eqs. (55) and (64), and those who need only the final GW spectrum may skip to Sec. IV.

### A. Notations

We first fix our notations and conventions used in the following argument. We denote the two spacetime points in the two-point correlator as (see Fig. 3 and 4)

$$x = (t_x, \vec{x}), \qquad y = (t_y, \vec{y}). \tag{28}$$

We sometimes use the time variables $(T, t_d)$ defined as

$$T \equiv \frac{t_x + t_y}{2}, \qquad t_d \equiv t_x - t_y, \tag{29}$$

instead of $(t_x, t_y)$. Also, we write their spacial separation as

$$\vec{r} \equiv \vec{x} - \vec{y}, \qquad r \equiv |\vec{r}|. \tag{30}$$

We often consider past light cones of $x$ and $y$, which are denoted by $S_x$ and $S_y$. The regions inside $S_x$ and $S_y$ are called $V_x$ and $V_y$, respectively, and we write their union as $V_{xy} \equiv V_x \cup V_y$. Since we consider bubbles with wall width $l_B$, we also define the spacetime points

$$x + \delta \equiv (t_x + l_B, \vec{x}), \qquad y + \delta \equiv (t_y + l_B, \vec{y}), \tag{31}$$

whose past light cones are denoted by $S_{x+\delta}$ and $S_{y+\delta}$, respectively. We also define the following regions

$$\delta V_x \equiv V_{x+\delta} - V_x, \qquad \delta V_y \equiv V_{y+\delta} - V_y, \tag{32}$$

whose intersection is denoted by

$$\delta V_{xy} \equiv \delta V_x \cap \delta V_y. \tag{33}$$

In addition, we define

$$\delta V_x^{(y)} \equiv \delta V_x - V_{y+\delta}, \qquad \delta V_y^{(x)} \equiv \delta V_y - V_{x+\delta}, \tag{34}$$

as shown in Fig. 3. Also, in Fig. 4, we show how Fig. 3 looks in $2+1$ dimensions.

On a constant-time hypersurface $\Sigma_t$ at time $t$, the two past light cones $S_x$ and $S_y$ form spheres, as shown in Fig. 5. We call these two spheres $C_x(t)$ and $C_y(t)$, whose centers are labeled by $O_x$ and $O_y$, respectively. The radii of $C_x(t)$ and $C_y(t)$ are given by

$$r_x(t) \equiv t_x - t, \qquad r_y(t) \equiv t_y - t. \tag{35}$$

These spheres $C_x(t)$ and $C_y(t)$ have an intersection for time $t < t_{xy}$ with

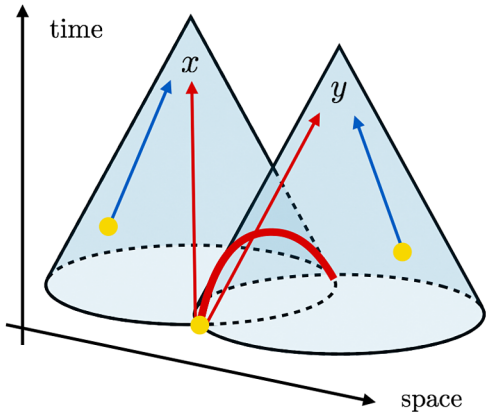


FIG. 4. How the light cones in Fig. 3 look like in $2+1$ dimensions. The yellow circles represent the nucleation points for single-bubble (on the red central arrows) and double-bubble (on the blue separate arrows) contributions. The red line along the intersection of the two light cones shows $\delta V_{xy}$ in Fig. 3.

$$t_{xy} \equiv \frac{t_x + t_y - r}{2}. \tag{36}$$

Let us consider arbitrary points $P_x(t)$ on $C_x(t)$ and $P_y(t)$ on $C_y(t)$. We denote unit vectors from $O_x$ and $O_y$ to $P_x(t)$ and $P_y(t)$ as $n_x(t)$ and $n_y(t)$, respectively. We parametrize these two unit vectors by the azimuthal and polar angles around $\vec{r}$ as

$$n_x \equiv (s_x c_{\phi x}, s_x s_{\phi x}, c_x), \qquad n_y \equiv (s_y c_{\phi y}, s_y s_{\phi y}, c_y), \tag{37}$$

where the label $t$ has been omitted for simplicity. Also, we use shorthand notations $c_x(s_x) \equiv \cos\theta_x(\sin\theta_x)$ $c_{\phi x}(s_{\phi x}) \equiv \cos\phi_x(\sin\phi_x)$ etc. in the following. We sometimes need to label an arbitrary point on the intersection of $C_x(t)$ and $C_y(t)$. We denote such point by $P(t)$, and also denote the unit vectors from $O_x$ and $O_y$ to $P(t)$ as $n_{x\times}(t)$ and $n_{y\times}(t)$, respectively. These unit vectors are parametrized by the azimuthal and polar angles $\theta_{x\times}(t)$, $\theta_{y\times}(t)$, $\phi_{x\times}(t)$ and $\phi_{y\times}(t)$ around $\vec{r}$. Especially, the cosines of the polar angles are given by

$$c_{x\times}(t) = \cos\theta_{x\times}(t) = -\frac{r_x(t)^2 + r^2 - r_y(t)^2}{2r_x(t)r}, \tag{38}$$

$$c_{y\times}(t) = \cos\theta_{y\times}(t) = \frac{r_y(t)^2 + r^2 - r_x(t)^2}{2r_y(t)r}. \tag{39}$$

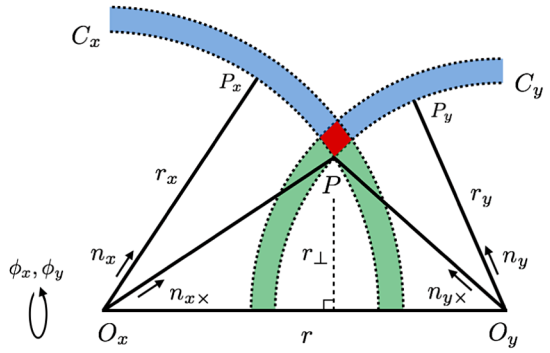


FIG. 5. Notations for quantities on the constant-time hypersurface $\Sigma_t$. The red diamond-shaped region denotes the one where a bubble nucleate in single-bubble spectrum (see Sec. III C), while the outer blue regions between the dotted lines denote the ones where bubbles nucleate in double-bubble spectrum (see Sec. III D).

## B. False vacuum probability

### 1. Probability for one point to remain in the false vacuum

For illustrative purpose, we first consider the probability $P(x)$ that a spacetime point $x$ is in the false vacuum. This occurs if and only if no bubbles are nucleated in $V_x$. Dividing $V_x$ into infinitesimal four-dimensional regions $dV_x^i$ so that $V_x = \cup_i dV_x^i$, one sees that the probability for no bubble to nucleate in $dV_x^i$ is given by $(1 - \Gamma dV_x^i)$. Thus $P(x)$ is written as [48]

$$P(x) = \prod_i (1 - \Gamma dV_x^i) = e^{-I(x)}, \tag{40}$$

with

$$I(x) = \int_{V_x} d^4z \Gamma(z). \tag{41}$$

### 2. Probability for two points to remain in the false vacuum

Next let us consider the probability $P(x,y)$ that given two points $x$ and $y$ both remain in the false vacuum. This probability is expressed in the same way as before

$$P(x,y) = e^{-I(x,y)}, \qquad I(x,y) = \int_{V_{xy}} d^4z \Gamma(z). \tag{42}$$

Below we require spacelike separation $r > |t_x - t_y|$, since only such configuration is relevant for the calculation of GW spectrum in the envelope approximation.[7] Then $I(x,y)$ is written as

$$I(x,y) = I_x^{(y)} + I_y^{(x)}, \tag{43}$$

[7]In the envelope approximation, it is impossible for two spacetime points $x = (t_x, \vec{x})$ and $y = (t_y, \vec{y})$ with timelike separation $t_x - t_y > r$ to be on bubble wall(s). This is because the spacial point $\vec{x}$ is caught up before $t = t_x$ by the bubble which passed through $y$.

$$I_x^{(y)} = \int_{-\infty}^{t_{xy}} dt \frac{\pi}{3} r_x(t)^3 \Gamma(t)(2 + c_{x\times}(t))(1 - c_{x\times}(t))^2 + \int_{t_{xy}}^{t_x} dt \frac{4\pi}{3} r_x(t)^3 \Gamma(t) \tag{44}$$

$$I_y^{(x)} = \int_{-\infty}^{t_{xy}} dt \frac{\pi}{3} r_y(t)^3 \Gamma(t)(2 - c_{y\times}(t))(1 + c_{y\times}(t))^2 + \int_{t_{xy}}^{t_y} dt \frac{4\pi}{3} r_y(t)^3 \Gamma(t). \tag{45}$$

Here we have different integrands for $t \in [-\infty, t_{xy}]$ and otherwise, because for the former the integration volume do not form complete spheres. The time integration can be performed to give

$$I(x, y) = 8\pi\Gamma(T)\mathcal{I}(t_d, r), \tag{46}$$

$$\mathcal{I}(t_d, r) = e^{t_d/2} + e^{-t_d/2} + \frac{t_d^2 - (r^2 + 4r)}{4r} e^{-r/2}, \tag{47}$$

where we have changed the variables from $(t_x, t_y)$ to $(T, t_d)$, and adopted $\beta = 1$ unit without loss of generality.

### C. Single-bubble spectrum

We now evaluate the single-bubble contribution to the correlator (18). With the envelope approximation, the following two conditions are required in order for a single bubble to give nonvanishing energy-momentum tensor at both $x$ and $y$:

(i) No bubbles are nucleated in $V_{xy}$.
(ii) At least one bubble is nucleated in $\delta V_{xy}$.

Note that the last condition reduces to "Only one bubble is nucleated in $\delta V_{xy}$" in the thin-wall limit $l_B \to 0$. Below, we briefly derive the GW spectrum via single-bubble contribution starting from these two conditions. The final expression is Eq. (55), and the details of the calculation are summarized in Appendix A.

From the above considerations, single-bubble contribution to the energy-momentum tensor is factorized in the following way ("$s$" denotes "single")

$$\langle T_{ij} T_{kl} \rangle^{(s)}(t_x, t_y, \vec{r}) = P(t_x, t_y, r) \int_{-\infty}^{t_{xy}} dt_n \Gamma(t_n) \times \int_{R_{xy}} d^3 z \mathcal{T}^{(s)}_{ij,kl}(t, t_x, t_y, \vec{r}), \tag{48}$$

where $R_{xy} \equiv \delta V_{xy} \cap \Sigma_{t_n}$ is the ring made by rotating the diamond-shape shown in Fig. 5 around the axis $\vec{r}$. Also, $\mathcal{T}^{(s)}_{ij,kl}$ is the value of $T_{ij}(x)T_{kl}(y)$ by the wall of the bubble nucleated at time $t_n$ (see Fig. 3 and 4). This is calculated as

$$\mathcal{T}^{(s)}_{ij,kl} = \left(\frac{4\pi}{3} r_x(t_n)^3 \cdot \kappa\rho_0 \cdot \frac{1}{4\pi r_x(t_n)^2 l_B}\right) \times \left(\frac{4\pi}{3} r_y(t_n)^3 \cdot \kappa\rho_0 \cdot \frac{1}{4\pi r_y(t_n)^2 l_B}\right) \times (N_\times(t_n))_{ijkl}, \tag{49}$$

with $(N_\times)_{ijkl} \equiv (n_{x\times})_i (n_{x\times})_j (n_{y\times})_k (n_{y\times})_l$. The integration by the nucleation time $t_n$ in Eq. (A3) can be performed explicitly, and after taking the projection $K$ in Eq. (18) into account, we have

$$K_{ij,kl}(\hat{k}) K_{ij,mn}(\hat{k}) \langle T_{kl} T_{mn} \rangle^{(s)}(t_x, t_y, \vec{r}) = \frac{2\pi}{9} \kappa^2 \rho_0^2 \Gamma(T) \frac{e^{-r/2}}{r^5} P(t_x, t_y, r) \times \left[\frac{1}{2} F_0 + \frac{1}{4}(1 - (\hat{r}\cdot\hat{k})^2) F_1 + \frac{1}{16}(1 - (\hat{r}\cdot\hat{k})^2)^2 F_2\right], \tag{50}$$

with $F$ functions given by

$$F_0 = 2(r^2 - t_d^2)^2 (r^2 + 6r + 12), \tag{51}$$

$$F_1 = 2(r^2 - t_d^2)[-r^2(r^3 + 4r^2 + 12r + 24) + t_d^2(r^3 + 12r^2 + 60r + 120)], \tag{52}$$

$$F_2 = \frac{1}{2}[r^4(r^4 + 4r^3 + 20r^2 + 72r + 144) - 2t_d^2 r^2 (r^4 + 12r^3 + 84r^2 + 360r + 720) + t_d^4 (r^4 + 20r^3 + 180r^2 + 840r + 1680)]. \tag{53}$$

Note that we have changed the time variables from $(t_x, t_y)$ to $(T, t_d)$. Also note that the correlator has now been successfully expressed analytically. Performing the integration over the angle between $\vec{r}$ and $\vec{k}$ in Eq. (18), we find

$$\Pi^{(s)}(t_x, t_y, k) = \frac{4\pi^2}{9} \kappa^2 \rho_0^2 \Gamma(T) \int_0^\infty dr \frac{e^{-r/2}}{r^3} P(t_x, t_y, r) \times \left[j_0(kr) F_0 + \frac{j_1(kr)}{kr} F_1 + \frac{j_2(kr)}{k^2 r^2} F_2\right]. \tag{54}$$

Then the integration over $T$ in Eq. (24) is performed by using the equality $\int_{-\infty}^{\infty} dY e^{-Xe^Y + nY} = (n-1)!/X^n$, and we obtain

$$\Delta^{(s)} = \frac{k^3}{12\pi} \int_0^\infty dt_d \int_{t_d}^\infty dr \frac{e^{-r/2}\cos(kt_d)}{r^3 \mathcal{I}(t_d, r)} \times \left[j_0(kr) F_0 + \frac{j_1(kr)}{kr} F_1 + \frac{j_2(kr)}{k^2 r^2} F_2\right], \tag{55}$$

where $j_{0,1,2}$ denote the spherical Bessel functions given in Appendix A.

### D. Double-bubble spectrum

Next we evaluate the double-bubble contribution to the correlator (18). With the envelope approximation, the following two conditions are necessary and sufficient for two different bubbles to give nonvanishing energy-momentum tensor at $x$ and $y$:

(i) No bubbles are nucleated in $V_{xy}$.
(ii) At least one bubble is nucleated in $\delta V_x^{(y)}$, and at least another is nucleated in $\delta V_y^{(x)}$.

Note that the last condition reduces to "Only one bubble is nucleated in each of $\delta V_x^{(y)}$ and $\delta V_y^{(x)}$" in the thin-wall limit $l_B \to 0$. Below we derive the GW spectrum via double-bubble contribution starting from these two conditions. The final result is given by Eq. (64).

From the above considerations, the two-bubble contribution to the energy-momentum tensor is decomposed as ("$d$" denotes "double")

$$\begin{aligned}
&\langle T_{ij}T_{kl}\rangle^{(d)}(t_x,t_y,\vec{r}) \\
&= P(t_x,t_y,r)\int_{-\infty}^{t_{xy}} dt_{xn}\Gamma(t_{xn}) \\
&\quad\times\int_{\delta V_x^{(y)}\cap\Sigma_{t_{xn}}} d^3x_n \mathcal{T}^{(d)}_{x,ij}(t_{xn},\vec{x}_n;t_x,\vec{r}) \\
&\quad\times\int_{-\infty}^{t_{xy}} dt_{yn}\Gamma(t_{yn}) \\
&\quad\times\int_{\delta V_y^{(x)}\cap\Sigma_{t_{yn}}} d^3y_n \mathcal{T}^{(d)}_{y,kl}(t_{yn},\vec{y}_n;t_y,\vec{r}),
\end{aligned} \tag{56}$$

where $\mathcal{T}^{(d)}_{x,ij}$ and $\mathcal{T}^{(d)}_{y,kl}$ are the value of the energy-momentum tensor by the bubble wall nucleated in $\vec{x}_n \in \delta V_x^{(y)}\cap\Sigma_{t_{xn}}$ and $\vec{y}_n \in \delta V_y^{(x)}\cap\Sigma_{t_{yn}}$ evaluated at the spacetime points $x$ and $y$, respectively. They are given by

$$\begin{aligned}
&\mathcal{T}^{(d)}_{x,ij}(t_{xn},\vec{x}_n;t_x,\vec{r}) \\
&\quad= \left(\frac{4\pi}{3}r_x(t_{xn})^3\cdot\kappa\rho_0\cdot\frac{1}{4\pi r_x(t_{xn})^2 l_B}\right)(n_x)_i(n_x)_j, \\
&\mathcal{T}^{(d)}_{y,kl}(t_{yn},\vec{y}_n;t_y,\vec{r}) \\
&\quad= \left(\frac{4\pi}{3}r_y(t_{yn})^3\cdot\kappa\rho_0\cdot\frac{1}{4\pi r_y(t_{yn})^2 l_B}\right)(n_y)_i(n_y)_j.
\end{aligned} \tag{57}$$

Here the arguments $t_{xn}$ and $t_{yn}$ in $n_x$ and $n_y$ are omitted for simplicity. Note that the time integration is over $[-\infty, t_{xy}]$ in Eq. (56), because the integration region $t_{xn} > t_{xy}$ or $t_{yn} > t_{xy}$ gives spherically symmetric contribution and thus vanishes (see Figs. 3–5, and notice that the nucleation points $P_x$ and $P_y$ run over the whole sphere for these nucleation times). Also note that the contribution to $x$ and that to $y$ factorize in Eq. (56) because the two bubbles nucleate independently of each other (see Figs. 3 and 4). There are no special directions except for $\vec{r}$, and therefore $\mathcal{T}^{(d)}_{z,ij}$ $(z = x, y)$ is decomposed as follows after integration over the nucleation time $t_{zn}$:

$$\begin{aligned}
&\int_{-\infty}^{t_{xy}} dt_{zn}\Gamma(t_{zn})\int d^3z_n \mathcal{T}^{(d)}_{z,ij}(t_{zn},\vec{z}_n;t_z,\vec{r}) \\
&\quad= \mathcal{A}_z^{(d)}(t_x,t_y,r)\delta_{ij} + \mathcal{B}_z^{(d)}(t_x,t_y,r)\hat{r}_i\hat{r}_j.
\end{aligned} \tag{58}$$

Here $\mathcal{A}_z^{(d)}$ and $\mathcal{B}_z^{(d)}$ depend on both $t_x$ and $t_y$ because the integration region for $z_n$ is affected by the other point. After the projection by $K$, only $\mathcal{B}$ component survives:

$$\begin{aligned}
&K_{ij,kl}(\hat{k})K_{ij,mn}(\hat{k})\langle T_{kl}T_{mn}\rangle^{(d)}(t_x,t_y,\vec{r}) \\
&\quad= \frac{1}{2}P(t_x,t_y,r)\mathcal{B}_x^{(d)}(t_x,t_y,r)\mathcal{B}_y^{(d)}(t_x,t_y,r)(1-(\hat{r}\cdot\hat{k})^2)^2.
\end{aligned} \tag{59}$$

Taking $\beta = 1$ unit without loss of generality, we can calculate $\mathcal{B}$ as

$$\mathcal{B}_x^{(d)}(t_x,t_y,r) = -\frac{\pi}{6}\kappa\rho_0\frac{e^{-r/2}}{r^3}\Gamma(T)G(t_d,r), \tag{60}$$

$$\mathcal{B}_y^{(d)}(t_x,t_y,r) = -\frac{\pi}{6}\kappa\rho_0\frac{e^{-r/2}}{r^3}\Gamma(T)G(-t_d,r), \tag{61}$$

with $G$ function given by

$$G(t_d,r) = (r^2-t_d^2)[(r^3+2r^2)+t_d(r^2+6r+12)]. \tag{62}$$

Note that we have now expressed the correlator analytically. As in the single-bubble case, the angular integration is readily calculated

$$\begin{aligned}
&\Pi^{(d)}(t_x,t_y,k) \\
&\quad= \frac{4\pi^3}{9}\kappa^2\rho_0^2\Gamma(T)^2\int_0^\infty drP(t_x,t_y,r)\frac{e^{-r}}{r^4} \\
&\qquad\times\frac{j_2(kr)}{k^2r^2}G(t_d,r)G(-t_d,r).
\end{aligned} \tag{63}$$

Substituting this into Eq. (24), and performing $T$ integration again by using the equality $\int_{-\infty}^{\infty} dY e^{-Xe^Y+nY} = (n-1)!/X^n$, we have

$$\Delta^{(d)} = \frac{k^3}{96\pi}\int_0^\infty dt_d \int_{t_d}^\infty dr \frac{e^{-r}\cos(kt_d)}{r^4\mathcal{I}(t_d,r)^2} \times \frac{j_2(kr)}{k^2r^2} G(t_d,r)G(-t_d,r). \quad (64)$$

## IV. NUMERICAL ESTIMATION

Since the remaining integrations in Eqs. (55) and (64) cannot be performed explicitly, we evaluate them numerically in this section.

In Fig. 6, the single- and double-bubble spectra $\Delta^{(s)}$ and $\Delta^{(d)}$ as well as their sum $\Delta = \Delta^{(s)} + \Delta^{(d)}$ are plotted. As seen from the figure, the low and high frequency behavior is

$$\Delta^{(s)} \propto \begin{cases} k^3 & (k/\beta \lesssim 1) \\ k^{-1} & (1 \lesssim k/\beta) \end{cases}, \quad (65)$$

$$\Delta^{(d)} \propto \begin{cases} k^3 & (k/\beta \lesssim 1) \\ k^{-1} & (1 \lesssim k/\beta \lesssim 10) \\ k^{-2} & (10 \lesssim k/\beta) \end{cases}. \quad (66)$$

Since $\Delta^{(s)}$ always dominates $\Delta^{(d)}$, their sum $\Delta$ behaves as

$$\Delta \propto \begin{cases} k^3 & (k/\beta \lesssim 1) \\ k^{-1} & (1 \lesssim k/\beta) \end{cases}, \quad (67)$$

and thus the high-frequency behavior in Ref. [37] is confirmed. Notice that we have restored $\beta$ in the expressions above.

Here we provide a fitting formula for the spectrum

$$\Delta = \frac{\Delta_{\rm peak}}{c_l(\frac{f}{f_{\rm peak}})^{-3} + (1-c_l-c_h)(\frac{f}{f_{\rm peak}})^{-1} + c_h(\frac{f}{f_{\rm peak}})}, \quad (68)$$

with $\Delta_{\rm peak} = 0.043$, $f_{\rm peak}/\beta = 1.2/2\pi \simeq 0.19$ and $(c_l, c_h) = (0.064, 0.48)$. Here "$l$" and "$h$" denote "low-frequency" and "high-frequency", respectively, and note that $f/f_{\rm peak} = k/k_{\rm peak}$. This formula reproduces the true spectrum within 8% error. The present spectrum is obtained by substituting Eq. (68) into Eq. (27), with $f_{\rm peak}$ given by the present value (26).

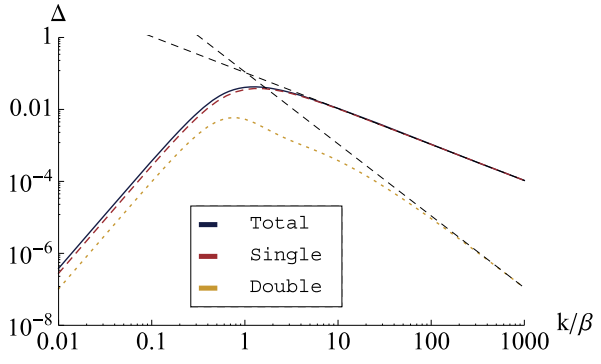


FIG. 6. Plot of the GW spectrum $\Delta$ (blue). Single- and double-bubble spectra $\Delta^{(s)}$ (red) and $\Delta^{(d)}$ (yellow) are also plotted. Black lines are auxiliary ones proportional to $k^{-1}$ and $k^{-2}$, respectively.

## V. FINITE VELOCITY

Though we have assumed luminal bubble walls in Secs. III–IV, we can easily generalize our results to an arbitrary value of the wall velocity. Just replacing parameters as $r_* \to r_*/v$ and $k \to vk$, we can estimate GWs in almost the same way as in the luminal case. As a result, we only have to replace the correlation function of the energy-momentum tensor as

$$\Pi(t_x, t_y, k) \to v^3\Pi(t_x, t_y, vk), \quad (69)$$

which means that the correlation function for $v \neq c$ is given by $\Pi = \Pi_v(t_x,t_y,k) = v^3\Pi_c(t_x,t_y,vk)$ with $\Pi_v$ and $\Pi_c$ being the correlation function in $v \neq c$ and $v = c$ case, respectively. Therefore we obtain

$$\Delta = \Delta^{(s)} + \Delta^{(d)}, \quad (70)$$

with

$$\Delta^{(s)} = \frac{v^3k^3}{12\pi}\int_0^\infty dt_d \int_{t_d}^\infty dr \frac{e^{-r/2}\cos(kt_d)}{r^3\mathcal{I}(t_d,r)} \times \left[j_0(vkr)F_0 + \frac{j_1(vkr)}{vkr}F_1 + \frac{j_2(vkr)}{v^2k^2r^2}F_2\right], \quad (71)$$

$$\Delta^{(d)} = \frac{v^3k^3}{96\pi}\int_0^\infty dt_d \int_{t_d}^\infty dr \frac{e^{-r}\cos(kt_d)}{r^4\mathcal{I}(t_d,r)^2} \times \frac{j_2(vkr)}{v^2k^2r^2} G(t_d,r)G(-t_d,r). \quad (72)$$

Note that all the quantities are normalized by $\beta$ in the expressions above.

As in the luminal case, it is difficult to proceed further in an analytical way, and hence we perform numerical calculation. Figure 7 is the plot of the GW spectrum $\Delta$ for $v = 1, 0.1$ and $0.01$ from top to bottom. The single- and double-bubble spectra are also shown in the same figure. From these plots one sees that $\Delta^{(d)}$ behaves $k^{-2}$ only for $v = c$, and in other cases $\Delta^{(s)}$ and $\Delta^{(d)}$ both behave as $\propto k^3$ and $\propto k^{-1}$ for low and high frequencies, respectively. This behavior is understood with the following Taylor expansion of $\Delta^{(d)}/v^3$ in terms of the wall velocity:

$$\frac{\Delta^{(d)}}{v^3} = \left(\frac{\Delta^{(d)}}{v^3}\right)^{(0)} + \left(1-\frac{v}{c}\right)\left(\frac{\Delta^{(d)}}{v^3}\right)^{(1)} + \cdots \quad (73)$$

Here note that all the terms vanish except for the first one for $v = c$. The next-leading term given by

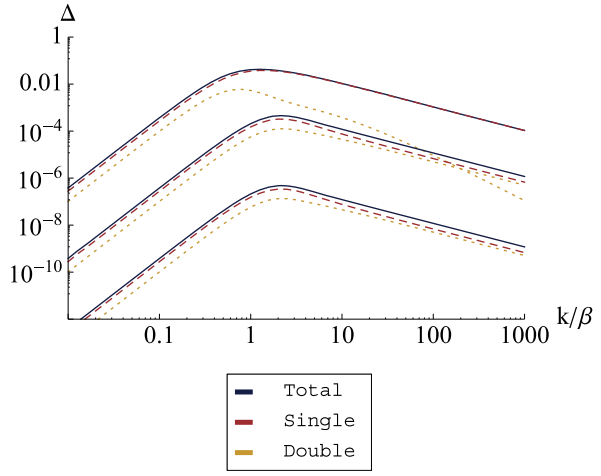


FIG. 7. Plot of the GW spectrum $\Delta$ (blue) for $v = 1$, 0.1 and 0.01 from top to bottom. Red and yellow lines correspond to single and double bubble spectrum $\Delta^{(s)}$ and $\Delta^{(d)}$, respectively.

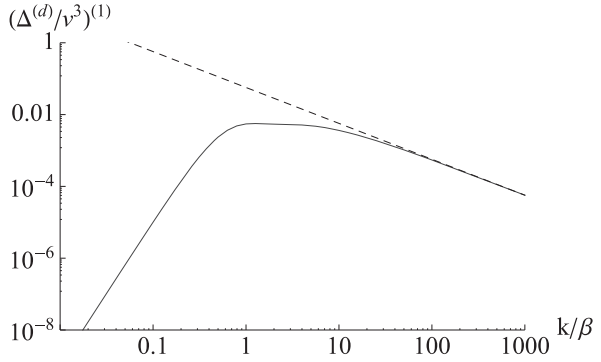


FIG. 8. Plot of the expansion coefficient $(\Delta^{(d)}/v^3)^{(1)}$ in Eq. (73) (blue) and an auxiliary line proportional to $k^{-1}$ (black). This figure shows that $(\Delta^{(d)}/v^3)^{(1)}$ scales as $k^{-1}$ for high frequencies.

$$\left(\frac{\Delta^{(d)}}{v^3}\right)^{(1)} = \frac{k^3}{96\pi}\int_0^\infty dt_d \int_{t_d}^\infty dr \frac{e^{-r}\cos(kt_d)}{r^4\mathcal{I}(t_d,r)^2} \times \frac{j_3(kr)}{k^2r^2} G(t_d,r)G(-t_d,r), \tag{74}$$

is plotted in Fig. 8, and it shows a clear $k^{-1}$ dependence in the high frequency region. This makes $\propto k^{-1}$ behavior in the spectra in Fig. 7 except for $v = c$. Our result is consistent with Ref. [37] qualitatively, and also quantitatively within a factor of 2.[8]

Finally we provide approximate formulas for the frequency and the spectrum at the peak, as well as the one for the present GW spectrum. The wall-velocity dependence of the peak frequency and amplitude is shown in Figs. 9–10 as blue lines, while the red lines are the following fitting formulas:

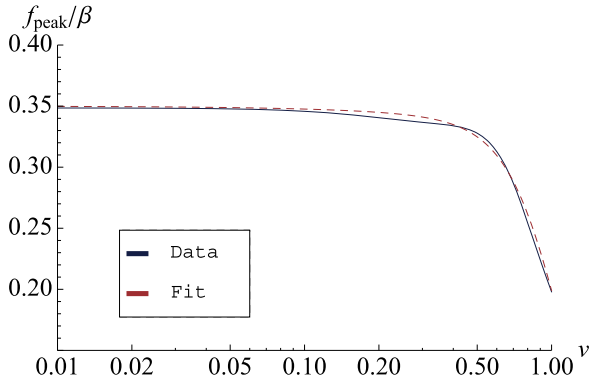


FIG. 9. Plot of the peak frequency $f_{\rm peak}/\beta$ as a function of the bubble wall velocity $v$. The blue line is numerically calculated from the analytic expression (71) and (72), while the red line corresponds to the fitting formula (75).

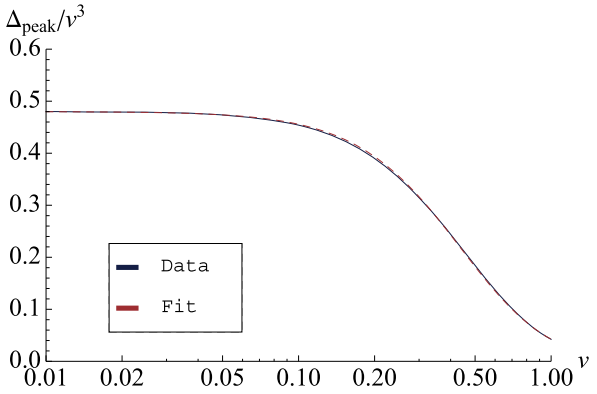


FIG. 10. Plot of the GW amplitude at the peak $\Delta_{\rm peak}$ scaled by $v^3$. The blue line is numerically calculated from the analytic expression (71) and (72), while the red line corresponds to the fitting formula (76).

$$\frac{f_{\rm peak}}{\beta} = \frac{0.35}{1 + 0.069v + 0.69v^4}, \tag{75}$$

$$\Delta_{\rm peak} = \frac{0.48v^3}{1 + 5.3v^2 + 5.0v^4}, \tag{76}$$

which reproduce the true peak and spectrum within 4% and 2% errors, respectively. The present peak frequency and amplitude are obtained by using Eqs. (26)–(27), which are shown here again

$$f = 1.65 \times 10^{-5}\ \text{Hz}\left(\frac{f_{\rm peak}}{\beta}\right)\left(\frac{\beta}{H_*}\right)\left(\frac{T_*}{10^2\ \text{GeV}}\right)\left(\frac{g_*}{100}\right)^{\frac{1}{6}}, \tag{77}$$

[8]We compared the fitting formulas (75) and (76) with those in Ref. [37].

$$\Omega_{\rm GW}h^2 = 1.67\times 10^{-5}\kappa^2\Delta_{\rm peak}\left(\frac{\beta}{H_*}\right)^{-2}\left(\frac{\alpha}{1+\alpha}\right)^2\left(\frac{g_*}{100}\right)^{-\frac{1}{3}}, \tag{78}$$

where $H_*$ and $T_*$ are the Hubble parameter at the transition and the temperature of the universe just after the transition, respectively, $g_*$ is the number of relativistic degrees of freedom at temperature $T_*$, $\kappa$ is the efficiency factor defined in Eq. (2), and $\alpha$ and $\beta$ are the fraction of the released energy density and the parameter in the nucleation rate defined in Eqs. (22) and (4), respectively.

## VI. DISCUSSION AND CONCLUSIONS

In this paper, we have derived analytical expressions for the gravitational wave (GW) spectrum from bubble collision during cosmological first-order phase transition, with thin-wall and envelope approximations in a flat background. [see Eqs. (55) and (64)]. The point is that we have only to know the two-point correlator of the energy-momentum tensor $\langle T(x)T(y)\rangle$, which in fact can be expressed in an analytic way. As a result, it is found that the most of the contributions to the spectrum come from single-bubble contribution to the correlator, and in addition the fall-off of the spectrum at high frequencies is found to be proportional to $f^{-1}$. We have also provided some fitting formulas for the spectrum [Eq. (68) and Eqs. (75)–(78)].

The key assumption which makes the analytic formulas quite simple is the thin-wall approximation, because this assumption enables us to classify various contributions to $\langle T(x)T(y)\rangle$ just as "single-bubble" and "double-bubble" in Sec. III. Therefore, it will be possible to extend our method to more general setups as long as we adopt the thin-wall approximation. For example, it may be possible to consider more general bubble nucleation rate or to include expansion of the universe. In addition, it is possible to calculate the GW spectrum analytically without the envelope approximation [43]. We leave such studies as future work.

## ACKNOWLEDGMENTS

The work of R. J. and M. T. is supported in part by Japan Society for the Promotion of Science (JSPS) Research Fellowships for Young Scientists.

## APPENDIX A: DETAILED CALCULATION OF THE SINGLE-BUBBLE SPECTRUM

In this appendix we show a detailed calculation of the single-bubble spectrum. The goal is to derive Eq. (55). The quantity we would like to calculate is

$$\Delta = \frac{3}{8\pi G}\frac{\beta^2\rho_{\rm tot}}{\kappa^2\rho_0^2}\Omega_{\rm GW} = \frac{3}{4\pi^2}\frac{\beta^2k^3}{\kappa^2\rho_0^2}\int dt_x\int dt_y\cos(k(t_x-t_y))\Pi(t_x,t_y,k). \tag{A1}$$

Below we take $\beta = 1$ unit without loss of generality. The function $\Pi$ is given by

$$\Pi(t_x,t_y,k) = K_{ij,kl}(\hat{k})K_{ij,mn}(\hat{k}) \times\int d^3r e^{i\vec{k}\cdot\vec{r}}\langle T_{kl}T_{mn}\rangle(t_x,t_y,\vec{r}), \tag{A2}$$

where $K_{ij,kl}$ denotes the projection given in Eq. (8). The single-bubble contribution to the two-point correlator of the energy-momentum tensor is decomposed as

$$\langle T_{ij}T_{kl}\rangle^{(s)}(t_x,t_y,\vec{r}) = P(t_x,t_y,r)\int_{-\infty}^{t_{xy}}dt_n\Gamma(t_n)\int_{R_{xy}}d^3z\mathcal{T}^{(s)}_{ij,kl}(t,t_x,t_y,\vec{r}), \tag{A3}$$

where $R_{xy}\equiv\delta V_{xy}\cap\Sigma_{t_n}$ is the ring made by rotating the diamond-shape shown in Fig. 5 around the axis $\vec{r}$. Also, $\mathcal{T}^{(s)}_{ij,kl}$ is the value of $T_{ij}(x)T_{kl}(y)$ by the wall of the bubble nucleated at time $t_n$ (see Figs. 3 and 4). This is calculated as

$$\mathcal{T}^{(s)}_{ij,kl} = \left(\frac{4\pi}{3}r_x(t_n)^3\cdot\kappa\rho_0\cdot\frac{1}{4\pi r_x(t_n)^2l_B}\right)\times\left(\frac{4\pi}{3}r_y(t_n)^3\cdot\kappa\rho_0\cdot\frac{1}{4\pi r_y(t_n)^2l_B}\right)\times(N_\times(t_n))_{ijkl}, \tag{A4}$$

with $(N_\times)_{ijkl}\equiv(n_{x\times})_i(n_{x\times})_j(n_{y\times})_k(n_{y\times})_l$. In the following we omit the argument $t_n$ in $r_x(t_n)$ and $r_y(t_n)$. Taking the projection operator $K$ into account, and noting that the area of the diamond in Fig. 5 is $l_B^2/\sin(\theta_x-\theta_y)$, we have

$$K_{ij,kl}(\hat{k})K_{ij,mn}(\hat{k})\langle T_{kl}T_{mn}\rangle^{(s)}(t_x,t_y,\vec{r}) = \left(\frac{\kappa\rho_0}{3}\right)^2P(t_x,t_y,r)\times\int_{-\infty}^{t_{xy}}dt_n\int d\phi\Gamma(t_n)\frac{r_x^2r_y^2}{r}K_{kl,mn}(N_\times)_{klmn}, \tag{A5}$$

Here we have used $r_xs_{x\times} = r_ys_{y\times}$ ($= r_\perp$ in Fig. 5), $-r_xc_{x\times}+r_yc_{y\times} = r$ and $K_{ij,kl}K_{ij,mn} = K_{kl,mn}$. Also, $\phi$ ($=\phi_{x\times}=\phi_{y\times}$ in Fig. 5) is the azimuthal angle around $\vec{r}$. Since there is no special direction except for $\vec{r}$, the correlator $\langle T_{ij}T_{kl}\rangle^{(s)}$ has only the following terms

$$\langle T_{ij}T_{kl}\rangle^{(s)} = a_1\delta_{ij}\delta_{kl}+a_2\frac{1}{2}(\delta_{ik}\delta_{jl}+\delta_{il}\delta_{jk}) + b_1\delta_{ij}\hat{r}_k\hat{r}_l+b_2\delta_{kl}\hat{r}_i\hat{r}_j + b_3\frac{1}{4}(\delta_{ik}\hat{r}_j\hat{r}_l+\delta_{il}\hat{r}_j\hat{r}_k+\delta_{jk}\hat{r}_i\hat{r}_l+\delta_{jl}\hat{r}_i\hat{r}_k) + c_1\hat{r}_i\hat{r}_j\hat{r}_k\hat{r}_l, \tag{A6}$$

with $a$, $b$ and $c$ denoting some coefficients. After projection, only a few terms survive:

$$K_{ij,kl}(\hat{k})K_{ij,mn}(\hat{k})\langle T_{kl}T_{mn}\rangle^{(s)} = 2a_2 + (1-c_{rk}^2)b_3 + \frac{1}{2}(1-c_{rk}^2)^2 c_1, \quad \text{(A7)}$$

with $c_{rk} \equiv \hat{r}\cdot\hat{k}$. Coefficients $a$, $b$, $c$ can be extracted by identifying $\vec{r}$ as $z$ direction

$$\begin{aligned}
&\langle T_{xx}T_{xx}\rangle^{(s)} = a_1 + a_2, \qquad \langle T_{xy}T_{xy}\rangle^{(s)} = \frac{1}{2}a_2,\\
&\langle T_{xx}T_{zz}\rangle^{(s)} = a_1 + b_1, \qquad \langle T_{zz}T_{xx}\rangle^{(s)} = a_1 + b_2,\\
&\langle T_{xz}T_{xz}\rangle^{(s)} = \frac{1}{2}a_2 + \frac{1}{4}b_3,\\
&\langle T_{zz}T_{zz}\rangle^{(s)} = a_1 + a_2 + b_1 + b_2 + b_3 + c_1, \qquad \text{(A8)}
\end{aligned}$$

which give

$$\begin{aligned}
a_2 &= 2\langle T_{xy}T_{xy}\rangle^{(s)},\\
b_3 &= 4(\langle T_{xz}T_{xz}\rangle^{(s)} - \langle T_{xy}T_{xy}\rangle^{(s)}),\\
c_1 &= \langle T_{xx}T_{xx}\rangle^{(s)} - (\langle T_{xx}T_{zz}\rangle^{(s)} + \langle T_{zz}T_{xx}\rangle^{(s)})\\
&\quad - 4\langle T_{xz}T_{xz}\rangle^{(s)} + \langle T_{zz}T_{zz}\rangle^{(s)}. \qquad \text{(A9)}
\end{aligned}$$

Therefore, we can write down the projected correlator as

$$\begin{aligned}
&K_{ij,kl}(\hat{k})K_{ij,mn}(\hat{k})\langle T_{kl}T_{mn}\rangle^{(s)}(t_x,t_y,\vec{r})\\
&= \left(\frac{\kappa\rho_0}{3}\right)^2 P(t_x,t_y,r)\int_{-\infty}^{t_{xy}} dt_n \int d\phi\,\Gamma(t_n)\frac{r_x^2 r_y^2}{r}\\
&\quad\times\Big[4N_{\times xy,xy} + 4(1-c_{rk}^2)(N_{\times xz,xz} - N_{\times xy,xy})\\
&\quad\times\frac{1}{2}(1-c_{rk}^2)^2(N_{\times xx,xx} - (N_{\times xx,zz} + N_{\times zz,xx})\\
&\quad - 4N_{\times xz,xz} + N_{\times zz,zz})\Big]\\
&= \frac{2\pi}{9}\kappa^2\rho_0^2 P(t_x,t_y,r)\int_{-\infty}^{t_{xy}} dt_n \Gamma(t_n)\frac{r_x^2 r_y^2}{r}\\
&\quad\times\left[\frac{1}{2}F_0' + \frac{1}{4}(1-c_{rk}^2)F_1' + \frac{1}{16}(1-c_{rk}^2)^2 F_2'\right] \qquad \text{(A10)}
\end{aligned}$$

with

$$F_0' = s_{x\times}^2 s_{y\times}^2, \qquad \text{(A11)}$$

$$F_1' = 8s_{x\times}c_{x\times}s_{y\times}c_{y\times} - 2s_{x\times}^2 s_{y\times}^2, \qquad \text{(A12)}$$

$$F_2' = 3s_{x\times}^2 s_{y\times}^2 - 4(s_{x\times}^2 c_{y\times}^2 + c_{x\times}^2 s_{y\times}^2) - 16s_{x\times}c_{x\times}s_{y\times}c_{y\times} + 8c_{x\times}^2 c_{y\times}^2. \qquad \text{(A13)}$$

Using $r_x s_{y\times} = r_y s_{y\times}$, we may arrange the expressions in the square parenthesis so that $s_{x\times}$ and $s_{y\times}$ appear only in $s_{x\times}^2$ and $s_{y\times}^2$:

$$\begin{aligned}
&K_{ij,kl}(\hat{k})K_{ij,mn}(\hat{k})\langle T_{kl}T_{mn}\rangle^{(s)}(t_x,t_y,\vec{r})\\
&= \frac{2\pi}{9}\kappa^2\rho_0^2 P(t_x,t_y,r)\int_{-\infty}^{t_{xy}} dt_n \frac{\Gamma(t_n)}{r}\\
&\quad\times\left[\frac{1}{2}F_0'' + \frac{1}{4}(1-c_{rk}^2)F_1'' + \frac{1}{16}(1-c_{rk}^2)^2 F_2''\right], \qquad \text{(A14)}
\end{aligned}$$

with

$$F_0'' = r_x^2 r_y^2 s_{x\times}^2 s_{y\times}^2, \qquad \text{(A15)}$$

$$F_1'' = r_x r_y[4c_{x\times}c_{y\times}(r_x^2 s_{x\times}^2 + r_y^2 s_{y\times}^2) - 2r_x r_y s_{x\times}^2 s_{y\times}^2], \qquad \text{(A16)}$$

$$F_2'' = r_x r_y[r_x r_y(19c_{x\times}^2 c_{y\times}^2 - 7(c_{x\times}^2 + c_{y\times}^2) + 3) - 8c_{x\times}c_{y\times}(r_x^2 s_{x\times}^2 + r_y^2 s_{y\times}^2)]. \qquad \text{(A17)}$$

This allows us to express the integrand without square roots coming from $s_{x\times} = \sqrt{1-c_{x\times}^2}$ etc.

Now the integration by the nucleation time $t_n$ can be performed explicitly by changing the integration variable from $t$ to $t_T \equiv t_n - T$. Here notice that $t_T$ integration is from $-\infty$ to $-r/2$ since $t_{xy} = T - r/2$. Also note that $F_0''$, $F_1''$ and $F_2''$ are polynomials in $t_T$ and that $\Gamma(t_n)$ can be factorized as $\Gamma(t_n) = \Gamma(T)e^{t_T}$. As a result, we obtain

$$\begin{aligned}
&K_{ij,kl}(\hat{k})K_{ij,mn}(\hat{k})\langle T_{kl}T_{mn}\rangle^{(s)}(t_x,t_y,\vec{r})\\
&= \frac{2\pi}{9}\kappa^2\rho_0^2 P(t_x,t_y,r)\Gamma(T)\frac{e^{-r/2}}{r^5}\\
&\quad\times\left[\frac{1}{2}F_0 + \frac{1}{4}(1-c_{rk}^2)F_1 + \frac{1}{16}(1-c_{rk}^2)^2 F_2\right], \qquad \text{(A18)}
\end{aligned}$$

with $F$ functions given by

$$F_0 = 2(r^2 - t_d^2)^2(r^2 + 6r + 12), \qquad \text{(A19)}$$

$$F_1 = 2(r^2 - t_d^2)[-r^2(r^3 + 4r^2 + 12r + 24) + t_d^2(r^3 + 12r^2 + 60r + 120)], \qquad \text{(A20)}$$

$$F_2 = \frac{1}{2}[r^4(r^4 + 4r^3 + 20r^2 + 72r + 144) - 2t_d^2 r^2(r^4 + 12r^3 + 84r^2 + 360r + 720) + t_d^4(r^4 + 20r^3 + 180r^2 + 840r + 1680)]. \qquad \text{(A21)}$$

In Eq. (A2) the integration by the angle between $\hat{r}$ and $\hat{k}$ is easily calculated, since the angular dependence appears only through $c_{rk}$. Noting that

$$\int_{-1}^{1} dc e^{icx} = 2j_0(x),$$
$$\int_{-1}^{1} dc e^{icx}(1-c^2) = \frac{4j_1(x)}{x},$$
$$\int_{-1}^{1} dc e^{icx}(1-c^2)^2 = \frac{16j_2(x)}{x^2}, \tag{A22}$$

with $j_i$ being the spherical Bessel functions

$$j_0(x) = \frac{\sin x}{x},$$
$$j_1(x) = \frac{\sin x - x\cos x}{x^2},$$
$$j_2(x) = \frac{(3-x^2)\sin x - 3x\cos x}{x^3},$$
$$j_3(x) = \frac{(15-6x^2)\sin x - (15x - x^3)\cos x}{x^4}, \tag{A23}$$

we have

$$\Pi^{(s)}(t_x, t_y, k) = \frac{4\pi^2}{9}\kappa^2\rho_0^2\Gamma(T)\int_0^\infty dr \frac{e^{-r/2}}{r^3} P(t_x, t_y, r) \times \left[j_0(kr)F_0 + \frac{j_1(kr)}{kr}F_1 + \frac{j_2(kr)}{k^2r^2}F_2\right]. \tag{A24}$$

Finally, let us consider the integration with respect to $T \equiv (t_1 + t_2)/2$ in Eq. (A1). Since $P(x, y)$ is given by [see Eq. (46)]

$$P(x, y) = e^{-8\pi\Gamma(T)\mathcal{I}(t_d, r)}, \tag{A25}$$

$T$ dependence of $\Pi^{(s)}(t_x, t_y, k)$ appears through the combination $\Gamma(T)e^{-8\pi\Gamma(T)\mathcal{I}(t_d,r)}$. By using the equality $\int_{-\infty}^{\infty} dY e^{-Xe^Y + nY} = (n-1)!/X^n$, the integration with respect to $T$ is performed analytically. After all, we have

$$\Delta^{(s)} = \frac{k^3}{12\pi}\int_0^\infty dt_d \int_{t_d}^\infty dr \frac{e^{-r/2}\cos(kt_d)}{r^3\mathcal{I}(t_d, r)} \times \left[j_0(kr)F_0 + \frac{j_1(kr)}{kr}F_1 + \frac{j_2(kr)}{k^2r^2}F_2\right]. \tag{A26}$$

## APPENDIX B: COMMENT ON "SPHERICAL SYMMETRY"

It is well known that spherically symmetric objects do not radiate gravitational waves. In this appendix we explain why this "spherical symmetry" argument does not undermine our calculation, especially the single-bubble contribution.

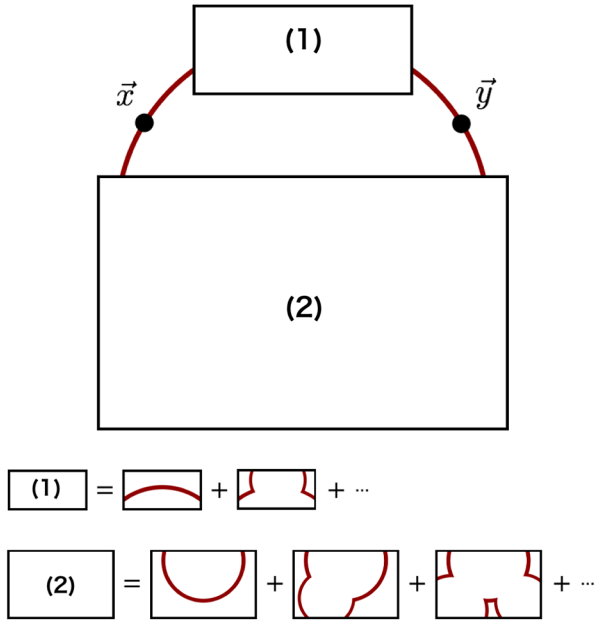


FIG. 11. Illustration of why the spherical symmetry of a single bubble do not undermine our argument. We set the evaluation time to be $t_x = t_y$ in this figure. We require the bubble walls fragments propagating to $\vec{x}$ and $\vec{y}$ to remain uncollided until the evaluation time, while other parts of this bubble can be already collided with others. This automatically takes into account the breaking of the spherical symmetry of a single bubble.

As is obvious from the derivation, our formalism, especially the single-bubble contribution, does not mean that the two evaluation points $\vec{x}$ and $\vec{y}$ are summed over the surface of a sphere. Instead, we first fix these evaluation points, and then sum over all the bubble configurations where the two bubble wall fragments originate from a single nucleation point. The very process of fixing $x$ and $y$ automatically takes into account the breaking of the spherical symmetry, because the parts of the bubble wall propagating toward the evaluation points are required to be uncollided until they reach these points, while no condition is imposed on other parts of the wall.

We illustrate this point in Fig. 11. Suppose we fix $x$ and $y$ so that $t_x = t_y$. Then, at this evaluation time, bubble walls in (1) and (2) regions remain uncollided and form part of a complete sphere in some cases (first terms in the R.H.S. of the equations), while in other cases they are already collided with other walls (the other terms in the same equations). On the other hand, the bubble wall fragments propagating toward $\vec{x}$ and $\vec{y}$ must remain uncollided until the evaluation time. Therefore, our formalism has nothing to do with the "spherical symmetry" argument, and automatically takes account of the breaking of the spherical symmetry by bubble collisions.

[1] A. A. Starobinsky, Spectrum of relict gravitational radiation and the early state of the universe, Pis'ma Zh. Eksp. Teor. Fiz. **30**, 719 (1979) [JETP Lett. **30**, 682 (1979)].
[2] S. Y. Khlebnikov and I. I. Tkachev, Relic gravitational waves produced after preheating, Phys. Rev. D **56**, 653 (1997).
[3] A. Vilenkin and E. P. S. Shellard, *Cosmic Strings and Other Topological Defects*, Cambridge Monographs on Mathematical Physics (Cambridge University Press, Cambridge, England, 2000).
[4] M. Gleiser and R. Roberts, Gravitational Waves from Collapsing Vacuum Domains, Phys. Rev. Lett. **81**, 5497 (1998).
[5] E. Witten, Cosmic separation of phases, Phys. Rev. D **30**, 272 (1984).
[6] C. J. Hogan, Gravitational radiation from cosmological phase transitions, Mon. Not. R. Astron. Soc. **218**, 629 (1986).
[7] J. R. Espinosa, T. Konstandin, J. M. No, and M. Quiros, Some cosmological implications of hidden sectors, Phys. Rev. D **78**, 123528 (2008).
[8] A. Ashoorioon and T. Konstandin, Strong electroweak phase transitions without collider traces, J. High Energy Phys. 07 (2009) 086.
[9] S. Das, P. J. Fox, A. Kumar, and N. Weiner, The dark side of the electroweak phase transition, J. High Energy Phys. 11 (2010) 108.
[10] L. Sagunski, DESY, Report No. DESY-THESIS-2013-011, http://inspirehep.net/record/1221682.
[11] M. Kakizaki, S. Kanemura, and T. Matsui, Gravitational waves as a probe of extended scalar sectors with the first order electroweak phase transition, Phys. Rev. D **92**, 115007 (2015).
[12] R. Jinno, K. Nakayama, and M. Takimoto, Gravitational waves from the first order phase transition of the Higgs field at high energy scales, Phys. Rev. D **93**, 045024 (2016).
[13] R. Apreda, M. Maggiore, A. Nicolis, and A. Riotto, Supersymmetric phase transitions and gravitational waves at LISA, Classical Quantum Gravity **18**, L155 (2001).
[14] R. Apreda, M. Maggiore, A. Nicolis, and A. Riotto, Gravitational waves from electroweak phase transitions, Nucl. Phys. **B631**, 342 (2002).
[15] J. Jaeckel, V. V. Khoze, and M. Spannowsky, Hearing the smoke of dark sectors with gravitational wave detectors, Phys. Rev. D **94**, 103519 (2016).
[16] S. J. Huber, T. Konstandin, G. Nardini, and I. Rues, Detectable gravitational waves from very strong phase transitions in the general NMSSM, J. Cosmol. Astropart. Phys. 03 (2016) 036.
[17] L. Leitao and A. Megevand, Gravitational waves from a very strong electroweak phase transition, J. Cosmol. Astropart. Phys. 05 (2016) 037.
[18] F. P. Huang, Y. Wan, D. G. Wang, Y. F. Cai, and X. Zhang, Probing the nature of the electroweak phase transition from particle colliders to gravitational wave detectors, Phys. Rev. D **94**, 041702 (2016).
[19] P. S. B. Dev and A. Mazumdar, Probing the scale of new physics by Advanced LIGO/VIRGO, Phys. Rev. D **93**, 104001 (2016).
[20] K. Hashino, M. Kakizaki, S. Kanemura, and T. Matsui, Synergy between measurements of the gravitational wave and the triple Higgs coupling in probing first order phase transition, Phys. Rev. D **94**, 015005 (2016).
[21] R. Jinno and M. Takimoto, Probing classically conformal $B-L$ model with gravitational waves, arXiv:1604.05035.
[22] K. Somiya (KAGRA Collaboration), Detector configuration of KAGRA: The Japanese cryogenic gravitational-wave detector, Classical Quantum Gravity **29**, 124007 (2012).
[23] F. Acernese *et al.* (VIRGO Collaboration), Advanced Virgo: a second-generation interferometric gravitational wave detector, Classical Quantum Gravity **32**, 024001 (2015).
[24] G. M. Harry (LIGO Scientific Collaboration), Advanced LIGO: The next generation of gravitational wave detectors, Classical Quantum Gravity **27**, 084006 (2010).
[25] P. A. Seoane *et al.* (eLISA Collaboration), The gravitational universe, arXiv:1305.5720.
[26] G. M. Harry, P. Fritschel, D. A. Shaddock, W. Folkner, and E. S. Phinney, Laser interferometry for the big bang observer, Classical Quantum Gravity **23**, 4887 (2006); Corrigendum, Classical Quantum Gravity **23**, 7361(E) (2006).
[27] N. Seto, S. Kawamura, and T. Nakamura, Possibility of Direct Measurement of the Acceleration of the Universe Using 0.1-Hz Band Laser Interferometer Gravitational Wave Antenna in Space, Phys. Rev. Lett. **87**, 221103 (2001).
[28] C. Caprini *et al.*, Science with the space-based interferometer eLISA. II: Gravitational waves from cosmological phase transitions, J. Cosmol. Astropart. Phys. 04 (2016) 001.
[29] A. Kosowsky, M. S. Turner, and R. Watkins, Gravitational radiation from colliding vacuum bubbles, Phys. Rev. D **45**, 4514 (1992).
[30] A. Kosowsky, M. S. Turner, and R. Watkins, Gravitational Waves from First Order Cosmological Phase Transitions, Phys. Rev. Lett. **69**, 2026 (1992).
[31] A. Kosowsky and M. S. Turner, Gravitational radiation from colliding vacuum bubbles: envelope approximation to many bubble collisions, Phys. Rev. D **47**, 4372 (1993).
[32] M. Kamionkowski, A. Kosowsky, and M. S. Turner, Gravitational radiation from first order phase transitions, Phys. Rev. D **49**, 2837 (1994).
[33] M. Hindmarsh, S. J. Huber, K. Rummukainen, and D. J. Weir, Gravitational Waves from the Sound of a First Order Phase Transition, Phys. Rev. Lett. **112**, 041301 (2014).
[34] J. T. Giblin and J. B. Mertens, Gravitional radiation from first-order phase transitions in the presence of a fluid, Phys. Rev. D **90**, 023532 (2014).
[35] M. Hindmarsh, S. J. Huber, K. Rummukainen, and D. J. Weir, Numerical simulations of acoustically generated gravitational waves at a first order phase transition, Phys. Rev. D **92**, 123009 (2015).
[36] D. J. Weir, Revisiting the envelope approximation: Gravitational waves from bubble collisions, Phys. Rev. D **93**, 124037 (2016).
[37] S. J. Huber and T. Konstandin, Gravitational wave production by collisions: More bubbles, J. Cosmol. Astropart. Phys. 09 (2008) 022.
[38] C. Caprini, R. Durrer, and G. Servant, Gravitational wave generation from bubble collisions in first-order phase transitions: An analytic approach, Phys. Rev. D **77**, 124015 (2008).

[39] C. Caprini, R. Durrer, T. Konstandin, and G. Servant, General properties of the gravitational wave spectrum from phase transitions, Phys. Rev. D **79**, 083519 (2009).
[40] C. Caprini and R. Durrer, Gravitational waves from stochastic relativistic sources: Primordial turbulence and magnetic fields, Phys. Rev. D **74**, 063521 (2006).
[41] G. Gogoberidze, T. Kahniashvili, and A. Kosowsky, The spectrum of gravitational radiation from primordial turbulence, Phys. Rev. D **76**, 083002 (2007).
[42] C. Caprini, R. Durrer, and G. Servant, The stochastic gravitational wave background from turbulence and magnetic fields generated by a first-order phase transition, J. Cosmol. Astropart. Phys. 12 (2009) 024.
[43] R. Jinno and M. Takimoto (to be published).
[44] P. J. Steinhardt, Relativistic detonation waves and bubble growth in false vacuum decay, Phys. Rev. D **25**, 2074 (1982).
[45] J. R. Espinosa, T. Konstandin, J. M. No, and G. Servant, Energy budget of cosmological first-order phase transitions, J. Cosmol. Astropart. Phys. 06 (2010) 028.
[46] A. D. Linde, On the vacuum instability and the Higgs meson mass, Phys. Lett. **70B**, 306 (1977).
[47] A. D. Linde, Decay of the false vacuum at finite temperature, Nucl. Phys. **B216**, 421 (1983); Erratum, Nucl. Phys. **B223**, 544 (1983).
[48] M. S. Turner, E. J. Weinberg, and L. M. Widrow, Bubble nucleation in first order inflation and other cosmological phase transitions, Phys. Rev. D **46**, 2384 (1992).